universität wien

MASTERARBEIT | MASTER'S THESIS

Titel | Title

Optical properties of WS_2@$ReSe_2$ nanotubules

verfasst von | submitted by

Vjosa Hoda

angestrebter akademischer Grad | in partial fulfilment of the requirements for the degree of

Master of Science (MSc)

Wien | Vienna, 2025

Studienkennzahl lt. Studienblatt | Degree programme code as it appears on the student record sheet:	UA 066 876
Studienrichtung lt. Studienblatt | Degree programme as it appears on the student record sheet:	Masterstudium Physics
Betreut von | Supervisor:	Univ.-Prof. Dr. Paola Ayala

Acknowledgements

First and foremost, I would like to thank my supervisor, Prof. Dr. Paola Ayala, for giving me the opportunity to work on this thesis and to explore such a fascinating topic in depth. Her encouragement and constant support have been very important to me throughout this journey. Her passion for research, and her dedication continue to inspire me every day.
I want to specially thank Vojtěch Kundrát for providing us the samples and for always being available for discussions. I am also thankful to Dido Denier van der Gon, BSc MSc, whose constant support and advice were very important throughout this project. I am deeply grateful for all the help, and kindness she has shown me along the way. I would also like to thank Ramon Pinna Brito, as well as all my colleagues from the THS group, for always being ready to help.
I owe my deepest gratitude to my family, my greatest blessing, for their endless love and never ending support throughout all these years. A very special thanks goes to my grandmother, to whom I dedicate this thesis, for her unconditional love, inspiration, and belief in my dreams.
I am very grateful to my loved one, Lundrim, for always believing in me, for his calmness, patience, and unconditional support throughout these very stressful and sleepless nights.
Finally, I would like to thank my dear fwend, Sissi, my lab buddy and one of the kindest people I have met during my studies, for her motivation, positivity, and continuous support. I am very grateful to call you my friend.
Thank you to everyone!

Abstract

The unique electronic and optical properties observed or expected from a plethora of two-dimensional materials have been the focus of intensive research in material science over the last two decades. Among these materials, transition metal dichalcogenides (TMDCs) take the lead by more than one reason. Not only their unique electronic, optical properties but also their catalytic properties make them useful in a wide range of applications, including flexible electronics, energy conversion, advanced sensors, and biomedical technologies. This Master Thesis focuses on the study of $ReSe_2$ and WS_2 tubular heterostructures, which can be bound to each other by van der Waals attraction and can be combined to form tubular heterostructures (WS_2@$ReSe_2$). These tubules do not mimic the properties of their 2D counterparts. Therefore, working with these new materials represents the development of new material properties that are not present in the individual layers. During my MSc work, I have aimed at investigating the optical and electronic properties of WS_2@$ReSe_2$ heterostructures, where WS_2 forms the inner nanotube and is wrapped by a $ReSe_2$ outer nanotube, creating a heterostructure. By combination of solid state spectroscopy techniques, I have consolidated a number of experimental results that provide information on relation and differences in the the structural characteristics of the TMDCs in question (WS_2 and $ReSe_2$) and their tubular heterostructures. It is important to mention that WS_2@$ReSe_2$ are relatively unexplored because we have used samples that have only recently been materialized.

To characterize these nanotubes, scanning electron microscopy (SEM) and energy-dispersive X-ray spectroscopy (EDS) were used to study their overall morphology and elemental composition, while Raman and photoluminescence (PL) spectroscopy were used to analyze their vibrational and optical properties. SEM images revealed rod-like nanotubes together with bulk and flake-like material, while EDS confirmed the presence of W, Re, S, and Se, consistent with the expected WS_2 and $ReSe_2$ composition. With Raman spectroscopy, we were able to observe the main vibrational modes of both WS_2 and $ReSe_2$ and compared them in mono-layered as well as bulk materials. These results were further compared with data available in the literature, and some small shifts could be identified and assigned to factors such as interlayer coupling and the curved geometry of the nanotubes. The PL results, showed emission peaks which differ significantly from the expected values for layered WS_2@$ReSe_2$ heterostructures (around 615 nm).
Despite a number of experimental challenges, the results here presented confirm the main elements and the vibrational features expected. Note that the spectroscopy part of these studies cannot be totally conclusive, since we need to continue working on the sample homogeneity. All in all, this study serves as a solid starting point for future research of WS_2@$ReSe_2$.

Kurzfassung

In den vergangenen zwei Jahrzehnten standen die einzigartigen elektronischen und optischen Eigenschaften zahlreicher zweidimensionaler Materialien im Zentrum der materialwissenschaftlichen Forschung. Eine besonders wichtige Rolle spielen dabei die sogenannten Übergangsmetall-Dichalkogenide (TMDCs). Aufgrund ihrer speziellen elektronischen, optischen und katalytischen Eigenschaften sind sie für ein breites Anwendungsspektrum interessant, das von flexibler Elektronik und Energieumwandlung bis hin zu fortschrittlicher Sensorik und biomedizinischen Technologien reicht.

In dieser Masterarbeit werden hohlzylindrische Heterostrukturen aus $ReSe_2$ und WS_2 untersucht, die durch van-der-Waals-Wechselwirkungen gebildet werden und sich zu WS_2@$ReSe_2$-Nanoröhren kombinieren lassen. WS_2 bildet dabei die innere Schicht und $ReSe_2$ die äußere Schicht der Nanoröhre. Aufgrund ihrer Krümmung, Anisotropie und geänderten Zwischenschichtkopplung besitzen solche Röhren andere Eigenschaften als planare 2D-Heteroschichten. Das Ziel bestand darin, die strukturellen, schwingungs- und optischen Merkmale dieser bislang kaum erforschten Systeme zu erfassen.

Zur Charakterisierung wurden Rasterelektronenmikroskopie (REM) und energiedispersive Röntgenspektroskopie (EDS) eingesetzt, um die Morphologie und die Elementzusammensetzung zu bestimmen. Ergänzend wurden die Raman- und die Photolumineszenz-(PL-)Spektroskopie genutzt, um die Schwingungs- und optischen Eigenschaften zu analysieren. Die REM-Aufnahmen zeigen überwiegend stabförmige Röhren sowie Begleitphasen in Schicht- und Pulverform. Die EDS-Analyse bestätigt die erwarteten Elemente W, Re, S und Se. In den Raman-Spektren lassen sich die Hauptmoden von WS_2 und $ReSe_2$ nachweisen. Kleinere Verschiebungen in diesen Graphen gegenüber Literaturwerten lassen sich mit veränderter Zwischenschichtkopplung und der gekrümmten Röhrengeometrie erklären. In der PL treten Emissionsmaxima auf, die deutlich von den für geschichtete WS_2@$ReSe_2$-Heterostrukturen unter 532-nm-Anregung typischerweise berichteten Werten um etwa 615 nm abweichen – ein bemerkenswertes Ergebnis, das sowohl die besondere Röhrenmorphologie als auch die experimentellen Randbedingungen (z. B. Anregungs-/Detektionsfenster) widerspiegelt und weitere Kontrollmessungen motiviert.

Trotz einzelner experimenteller Herausforderungen (u. a. Probenhomogenität, Instrumentstabilität) bestätigen die Ergebnisse die wesentlichen strukturellen und schwingungsspektroskopischen Merkmale der untersuchten Materialien. Insgesamt bildet die Arbeit eine stabile Grundlage für zukünftige Studien an WS_2@$ReSe_2$-Nanoröhren und zeigt, dass röhrenförmige TMDC-Heterostrukturen Eigenschaften ermöglichen, die in planaren Schichtsystemen nicht realisierbar sind.

Contents

List of Figures

1. Introduction

1.1. Motivation

The development of new materials is a major focus of research in many scientific fields. Materials designed for energy and semiconductor applications are important, which is why creating compounds with tailored properties has become a central goal in modern materials science. The aim of this thesis is to study the optical and vibrational properties of WS_2@$ReSe_2$ heteronanotubes. These are multilayered tubular structures consisting of an inner core of WS_2 and an outer shell of $ReSe_2$. Since they are newly developed, their physical properties are still mostly unknown.
The research on these materials has been largely inspired by the important investigations of the last two, or even three, decades. Two-dimensional (2D) materials have become an important area of research because of their unique electronic and optical properties. Among them, transition metal dichalcogenides (TMDCs) such as $ReSe_2$ and WS_2 are especially promising. When these materials are combined through van der Waals interactions, they can form heterostructures like WS_2@$ReSe_2$, which show new properties not found in the individual layers. This thesis explores the optical properties of WS_2@$ReSe_2$ heterostructures with a special core-shell design, where WS_2 forms the inner nanotube and $ReSe_2$ forms the outer shell. This layered arrangement allows the two materials to interact closely while still keeping their own characteristics. Such structures make it possible to tune band alignment, create interlayer excitons, and control charge transfer, all of which are important for applications in optoelectronics, photocatalysis, and quantum technologies. Overall, this work is an initial step toward understanding WS_2@$ReSe_2$ heteronanotubes and highlights their potential for future applications in advanced electronic and optical devices.

1.2. 1D and 2D Hybrids of Transition Metal Dichalcogenides

Two-dimensional materials represent an exciting part in modern science and technology, offering unique properties that materials show when thinned to atomic layers. The discovery of graphene - a single layer of carbon atoms, opened new doors for material research and shows how the properties of a material change when going to the nanoscale. Although graphene has shown incredible electrical and mechanical properties, it lacks a bandgap, which limits its usage in semiconductor devices. This was the main reason why TMDCs were brought to attention.[1] [9] TMDCs, as well as graphene, represent a remarkable class of materials that have a two-dimensional (2D) configuration, which are promising semiconductors. These TMDC materials are semiconductors of type MX_2,

where M is a transition metal such as molybdenum (Mo), tungsten (W), rhenium, (Re) and X is a chalcogen atom such as sulfur (S), selenium, (Se) and tellurium (Te), where one layer of M atoms is sandwiched between two layers of X atoms.[9]
TMDCs can form different structures depending on how the transition metal atoms are surrounded. The two most common structures are 2H where the metal atoms are arranged in a trigonal primatic shape. In the 2H phase, the layers follow an ABA stacking order, where the top and bottom chalcogen atoms align directly on top of each other. The other structure is 1T where the metal atoms are arranged in an octahedral shape. In the 1T phase, the stacking follows an ABC order, where each layer is shifted relative to the one below. Which phase is stable depends on the combination of the metal M and the chalcogen X.[9]

One of the most interesting properties about TMDCs is their thickness-dependent electronic properties. In bulk form, TMDCs have an indirect band gap, whereas in monolayer form, for most TMDCs the gap becomes direct, enabling efficient light absorption and emission in the visible range, which makes them ideal for optoelectronic devices.[10] In addition to this monolayer TMDCs show strong spin-orbit coupling, leading to spin-valley coupling.[9]
Synthesis of TMDCs can be done using chemical methods such as: the chemical vapor deposition (CVD), molecular beam epitaxy (MBE) and metal-organic CVD. The one that is mostly used because it is more practical is the chemical vapor deposition (CVD). It is cheaper and easier to use since it does not require ultra-high vacuum. There are also physical methods for the synthesis of TMDCs, like Physical Vapor Deposition (PVD), pulsed laser deposition (PLD) etc. [11]
Although layered TMDCs have received considerable attention in recent years, researchers also discovered that these materials can have tubular counterparts, similar to carbon nanotubes. However, single-walled TMDC nanotubes are difficult to produce because they require high temperatures and often result in mixed or impure products. More recently, gold nanoparticles have been used as catalysts to grow longer and more uniform TMDC nanotubes, reaching lengths up to half a millimeter for the WS_2 nanotubes. These nanotubes are very strong, with a high Young's modulus (160–179 GPa) and can stretch over 10% before breaking, making them useful for reinforcing materials like plastics.[12]

1.3. State-of-the-art

TMDCs have become a key focus in materials science because of their properties.[13, 14] These materials consist of layers where transition metal atoms are sandwiched between chalcogen atom layers in a hexagonal structure.[14, 15, 16] A unique feature of TMDCs is their strong tenability, since their properties can be changed by changing layer thickness, chemical composition, or applying external force.[17, 18, 19]
TMDCs are seen as great materials for optoelectronics, as they show strong light–matter interactions, tunable bandgaps, and efficient light emission.[20, 21] These properties make it possible for them to be used in photodetectors, LEDs, and solar cells. Quantum

confinement and excitonic effects in monolayer TMDCs also allow for the development of ultra-compact, high-performance photonic and quantum devices.[22, 23, 24]
In electronics, TMDCs are considered promising materials for many types of devices. They have high charge mobility, good control over electric fields, and are flexible, which makes them ideal for thin and transparent electronic systems.[25, 26] Bulk TMDCs usually have an indirect bandgap, but when thinned to a single layer, many switch to a direct bandgap, which improves their optical response. Some TMDCs, like $MoTe_2$, can even change from semiconducting to metallic as the number of layers decreases.[27, 28]
Besides electronics and optics, TMDCs are also useful in batteries, supercapacitors, and water-splitting systems because of their stability. They can act as sensitive sensors for gases, biomolecules, and mechanical strain, making them important in medicine and different industrial fields.[26, 29, 30, 31]
TMDC nanotubes have practical applications in different fields. They can strengthen plastics and polymers, making them useful for medical devices and automotive parts. In energy, they are promising as materials for lithium-ion batteries and fuel cell membranes. WS_2 nanotubes can speed up reactions that break down pollutants, and they can also help split water to make hydrogen fuel. More recently, researchers have discovered unique optoelectronic applications, including programmable memory devices and ferroelectric devices that combine data storage with mechanical and optical functions.[12]
Depending on their composition and doping, TMDCs can act as either n-type or p-type semiconductors. Materials like MoS_2 and WS_2 are usually n-type semicoundtors used in different electronic devices. Materials like WSe_2 and $ReSe_2$ usually show p-type semiconductors which are used for logic circuits.[32, 33, 34] This is just a brief overview compared to the tremendous amount of research currently carried out with materials of this class.

1.4. Specific scope of this Master Thesis

This thesis focuses on a recently developed material that has been obtained in our group via a collaboration with the groups of Prof.Vojtěch Kundrát, at Masaryk University in the Czech Republic and Prof. Reshef Tenne at the Weizmann Institute in Israel. This materials consists on transition metal dichalcogenides TMDCs in their nanotube form as described in the chapters to follow. In particular, WS_2@$ReSe_2$ heteronanotubes are studied. Since these are completely new materials, to the best of my knowledge, they have not been previously investigated within the spectroscopy point of view performed within my MSc work. Even their layered counterparts, the WS_2@$ReSe_2$ heterostructures, have been rarely studied.

Briefly, this Master Thesis summarizes the work I have carried out to study the optical and vibrational properties of WS_2@$ReSe_2$ heteronanotubes to gain a deeper understanding of their structure and behavior. The next chapter introduces the basic theory of TMDCs, which helps to understand the spectroscopy results presented later. The following chapters describe the experimental methods used for characterization and discuss the obtained results. Finally, potential questions and ideas for future research are purposed. The goal

of this study is to take the first steps toward a better understanding of TMDC nanotube heterostructures, while recognizing that further research will be needed to fully explore their fascinating physical properties.

2. Theoretical background

This chapter provides the general background of transition metal dichalcogenides (TMDCs) and why they are important, with a focus on two dimensional transition metal dichalcogenides (TMDCs) and their nanotube form. It gives a brief overview of both WS_2 and $ReSe_2$, both in their layered structure and as nanotube, and briefly explains the approaches used for synthesis of TMDC nanotubes. Additionally, this chapter includes the physical principal behind the main techniques used for the analysis, including Raman spectroscopy, photoluminescence spectroscopy (PL), scanning electron microscopy (SEM) and energy dispersive X-ray spectroscopy (EDS).

2.1. Transition metal dichalcogenides (TMDCs)

2.1.1. 2D TMDC

Transition metal dichalcogenides (TMDCs) are two dimensional (2D) layered materials that show outstanding electronic and optical properties. These materials have attracted a lot of interest due to their unique physical properties that differ from those of the bulk material. These materials, composed of three atomic planes containing a transition metal sandwiched between two chalcogen atoms, show a unique combination of structural, electronic, and optical properties that make them highly promising for next-generation optoelectronic applications.[9] [1]

The general formula for TMDCs is MX_2, where M is a transition metal such as molybdenum (Mo), tungsten (W), rhenium (Re), and X is a chalcogen atom such as sulfur (S), selenium (Se), and tellurium (Te), that form an interesting class of layered semiconductors.[35] [9] An example of a layered TMDC is given below in figure 2.1. Unlike graphene, which lacks a bandgap, many TMDCs exhibit direct or indirect sizable bandgaps, which provide promising alternatives for photodetectors, electroluminescent devices and transistors.[9] [1]

TMDCs consist of sandwich-like layers in which an atom of a transition metal is bound to two chalcogen atoms. TMDCs are bound to each other by van der Waals attraction and can be combined to form heterostructures, such as (WS_2@$ReSe_2$), that allow the development of new material properties that are not present in the individual layers. A very interesting feature of TMDCs is their layer-dependent properties. While bulk TMDCs exhibit indirect bandgap, most monolayer TMDCs exhibit direct bandgap which makes them ideal for optoelectronic devices.[10] In addition to their monolayer and bulk forms, TMDCs can also be stacked to form van der Waals heterostructures, which enable tailored band alignments and interlayer interactions. An interesting example is the type-II WS_2–$ReSe_2$ heterostructure, which has a special band alignment that helps

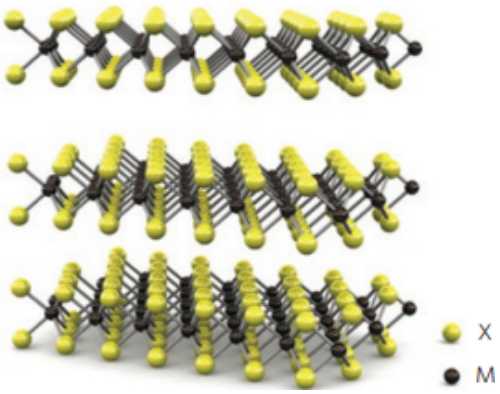

Figure 2.1.: Schematic representation of XM_2 structure, where M is a transition metal and X is a chalcogen atom [1]

separate charges between the two layers.[5] Absorption measurements show that holes transfer from WS_2 to $ReSe_2$ layer very fast and also electrons transfer from $ReSe_2$ to WS_2, a phenomena seen in Figure 2.6 . These observations show that WS_2 and $ReSe_2$ form a type-II heterostructure.[5][36] The spatial separation of electrons and holes in type-II heterostructures gives rise to interlayer excitons, where the electron and hole are spatially separated into different layers.[36] These charge-transfer effects show why TMDC heterostructures are promising for devices such as photodetectors and solar cells, where fast and efficient separation of charges is needed.[5]

Type-I and Type-II band alignment

In van der Waals heterostructures composed of different TMDC monolayers, the positions of the conduction and valence bands determine how carriers are distributed between the layers. This relationship is referred to as the band alignment, and two common cases are Type-I and Type-II.[37]

In a **Type-I band alignment**, the conduction band minimum (CBM) and the valence band maximum (VBM) of one material are both inside the bandgap of the other, as seen in Figure 2.2a. This means that electrons and holes end up in the same layer, which makes recombination easier. Such an alignment is useful for light-emitting applications.[37]

In a **Type-II band alignment**, the conduction band minimum (CBM) and the valence band maximum (VBM) are in different materials. Here, electrons move into the material with the lower CBM, while holes stay in the material with the higher VBM, as seen in Figure 2.2b. Because the charges are separated into different layers, recombination is reduced and carrier lifetimes become longer. This makes Type-II structures important for photovoltaic devices and photodetectors, where efficient charge separation is important.[37]

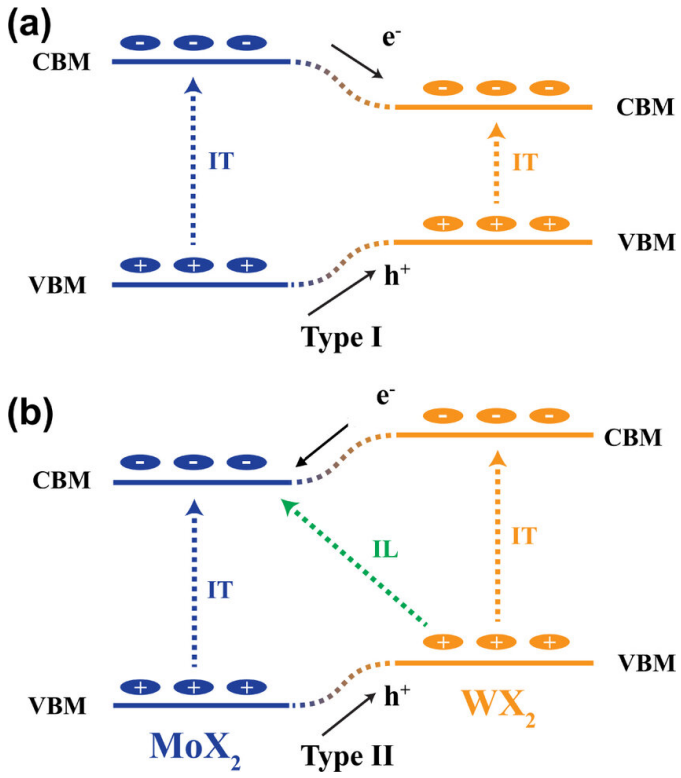

Figure 2.2.: a). Type-I band alignment and b).Type-II band alignment
IT indicates intralayer and interlayer optical transitions[2]

2.1.2. TMDC nanotubes

Although layered TMDCs have been the focus of researchers lately, after the discovery of carbon nanotubes, a new hypothesis was given to fold these inorganic 2D materials to form nanotubes.[12]. Even though they were discovered imidiately after carbon nanotubes, they didn't get alot of attention and the main reason for that is that single walled nanotube TMDCs with well defined chiral angles are much harder to produce. To make this nanotubes high temperature reactions are needed, and even in those cases it doesn't mean that we would get pure nanotubes.[12]

Progress has been made in the synthesis of multiwalled nanotubes, making it possible for the synthesis of these nanotubes using classical chemical vapor deposition (CVD) reactor and vapor-liquid-solid (VLS) growth mode. WS_2 nanotubes form from sulfidation of tungsten oxide nanoparticles $(WO_{3-x})/W_{18}O_{49}$ nanowhiskers, can be exposed to sulfur vapors and hydrogen and work its way inward layer by layer untill a hollow nanotube is formed. In the beginning the first layers are formed fast in temperature 840 °C, but for the layers in the inner part waiting for a few hours is needed for the process to finish.[12] One recent way to grow more uniform TMDC nanotubes is by using gold nanoparticles as catalists, and these nanotubes can be very long, up to half milimeter in length, specifically

for WS_2.
Transition metal dichalcogenides show impressive mechanical properties. They have Young's modulus between 160-179GPa, which means they are very stiff and can undergo a lot of stress before breaking. Also they strech for more than 10% before breaking, which means they can be used to strengthen materials such as plastic. TMDC nanotubes can be synthesized with different diameters and lengths. An SEM image of a TMDC nanotube can be seen in Figure 2.3. In addition, depending on the nanotube size, they interact with light differently. Smaller tubes show exciton behavior, larger nanotubes (above ∼60nm) act like optical resonators, creating states exciton-polaritons. On the other hand, mechanical properties can be changed. If mechanical stress is applied, it can change its bandgap.[12]

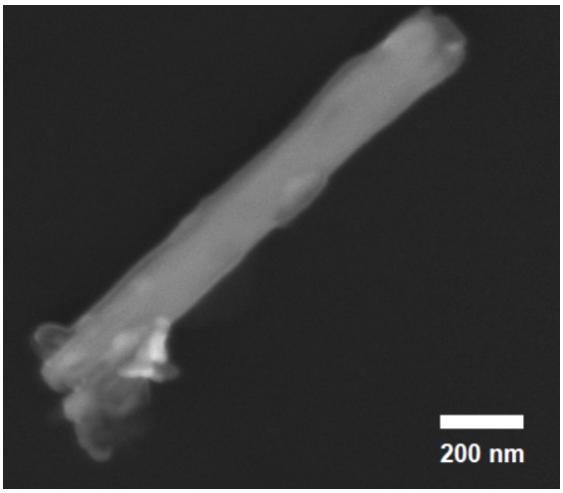

Figure 2.3.: SEM image of a nanotubes

TMDC nanotubes can have applications in various fields. One application is photovoltaic random-access memory, where individual nanotubes can store imformation optically and electrically at the same time. This works because when you apply voltage to these multiwall tubes, the inner and outer layers slide move a little against each other, creating an electric dipole that stays in place even after removing the power. These nanotubes also can be used as electrode materials in lithium-ion batteries because their hollow structure is good pathways for lithium ions to move in and out during charging and discharging cycles. TMDC nanotubes also are very good making materials stronger when mixed into polymers, creating stronger and tougher plastics suitable for automotive parts and medical devices. Even though WS_2 nanotubes have many promising uses, it is still difficult for researchers to fully control how they grow, especially their chirality and diameter.[6] [12]

2.2. Nanostructures of WS_2 and $ReSe_2$

From the chemical point of view, understanding the bonding environments WS_2 and $ReSe_2$ can provide important insights to the properties of their tubular counterparts. Some of their properties can be inferred from the 2D materials but it is to interpret the behavior of their heterostructured combinations taking additional information into account. This section reviews briefly what is known for the 2D materials and an explanation to what is expected for the nanotubes is described.

2.2.1. WS_2 nanostructures

Tungsten disulfide is a two dimensional material, made of W atoms sandwiched between two layers of S atoms. It is composed of three different structures, hexagonal (2H), trigonal (1T) or rhombohedral (3R) phase. Tungsten disulfide crystallizes primarily in the hexagonal 2H phase, which is more stable under ambient conditions.[38] The crystal structure consists of hexagonal tungsten atoms arranged between two layers of hexagonal arranged sulfur atoms, forming the characteristic sandwich structure typical of group VI TMDCs. The interlayers of WS_2 are bound by van der Waals forces, with an distance between the layers of ∼0.6 nm.[39][38]
WS_2 has unique layer-dependent properties, including strong light absorption of 5–10% of incident sunlight, as well as band structure. The electronic properties of WS_2 show a strong dependence on the layer thickness, which is common for TMDCs in general. Similar to MO_2, bulk 2H WS_2 is a semiconductor with an indirect bandgap of around 1.3eV. On the other hand, monolayer 2H WS_2 has a direct bandgap of around 1.98 eV.[38] This indirect-to-direct bandgap transition can be attributed to the quantum confinement effects and changes in the electronic band structure when the material is reduced to monolayer thickness.[40][38] The monolayer of WS_2 shows a strong PL peak at around 1.98 eV (∼626 nm), while the peak corresponding to the structure has a small shift at 1.95 eV (∼635 nm) and it has much weaker intensity. The decrease in PL intensity and the shift of the peak are related to layer number, carrier and concentration. These results confirm that the WS_2 monolayer has a direct band gap.[38] Additionally, for single layer WS_2, the main Raman peaks for WS_2 have been observed at ∼357.2 cm^{-1} for the ${E_{2g}}^1$ and ∼418.6 cm^{-1} for the A_{1g}. As the number of WS_2 layers increases, the ${E_{2g}}^1$ peak shifts to lower frequency (red shift) and the A_{1g} peak shifts to higher frequency (blue shift). As a result, the separation between the two peaks increases until it reaches a constant value in the bulk limit.[41] When excited with different lasers, more first and second order modes can be observed. For example, when excited with 488nm, the most dominant peaks are the first order modes, ∼355.9 cm^{-1} (E12g) and ∼417.5 cm^{-1} (A1g). When excited with the 515nm, more second order modes appear, with main peaks at ∼355.2 cm^{-1} (${E_{2g}}^1$) and ∼417.2 cm^{-1} (A_{1g}).[42]

The behavior of TMDC nanostructures differ based on their shape (flat sheets, fullerene like particles or nanotubes), and it also changes with size, number of layers and chirality. The same 2D material explained above, can also be found in one dimensional form, as a nanotube, Figure 2.4. In 1992, fullerene like structures and nanotubes of WS_2 were first

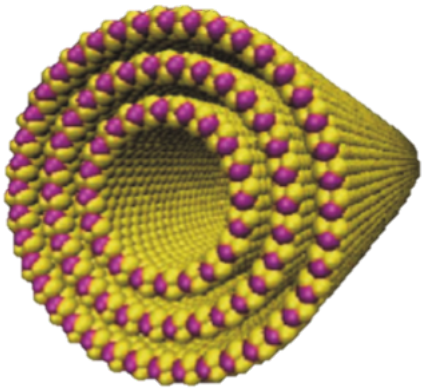

Figure 2.4.: WS_2 multi-walled nanotube[3]

synthesized, and not long after, also MoS_2 was reported by Reshef Tenne and coworkers. Tenne has prepared the WS_2 and MoS_2 nanotubes by heating WO_3 or MoO in $H_2S/H_2/N_2$ gas atmosphere at a temperature around 850 °C. To this day different methods are used to synthesize these kind of nanotubes.[43][44]
Furthermore, TMDC nanotubes can be synthesized by converting transition metal oxide nanowires through sulfurization. By reducing the diameter of the oxide nanowires, small-diameter nanotubes with few walls can be synthesized. Recent studies have reported nanotubes as small as 8–25 nm, showing that this method is very promising for making high-quality TMDC nanotubes. In a recent study, it was made possible to synthesize nanotubes by chalcogenizing structure-controlled tungsten oxide nanowires grown via CVD. This method has shown that nanotubes with inner diameter of $\sim 6 \pm 3$ nm and $\sim 5 \pm 2$ nm walls can be synthesized.[45]

The optical and electronic properties of TMDC nanotubes have recently been studied in detail. WS_2 nanotubes were found to become superconducting at very low temperatures (around 5.8 K) and showed special quantum effects such as Little–Parks oscillations. Other important discoveries include strong coupling between light in optical cavities and excitons in MoS_2 and WS_2 nanotubes, nonlinear effects such as second harmonic generation, and sliding ferroelectricity that can be used for optical data storage. WS_2 nanotubes have been used also to build self-sensing nanodevices.[46]
In addition, Raman studies have shown layer dependent behavior of WS_2 nanotubes. The results show that WS_2 nanotubes can have the same outer diameter but a different number of wall layers depending on the sulfurization time. Longer sulfurization increases the number of WS_2 layers inside the nanotube without changing its diameter. Raman spectroscopy for the nanotube form of the WS_2, shows again two main vibration modes, the in-plane ${E_{2g}}^1$ mode at around 352 cm^{-1} and the interlayer A_{1g} mode at around 420 cm^{-1}, where both peaks become stronger with longer sulfurization. Interestingly, the A_{1g} mode is more intense than the ${E_{2g}}^1$ mode, unlike in monolayer WS_2 sheets. In a research made recently it has been shown that for smaller nanotubes (about 8 nm in diameter), the A_{1g} peak shifted from 420.5 cm^{-1} to 418.0 cm^{-1} as the sulfurization time increased

to 25 minutes, and for larger nanotubes (25 nm in diameter) the peak stayed constant at 420.5 cm^{-1}. This red shift in smaller nanotubes it can be due to curvature-induced strain, which reduces the interlayer vibration frequency, whereas van der Waals forces between layers tend to strengthen it.[47]

The synthesis of WS_2 is usually done through sulfidation of nanoparticles of WO_{3-x}, at a high temperature (>800 °C). First, the oxide partly reduces and forms $W_{18}O_{49}$ nanowhiskers, which can easily evaporate, especially in the presence of water molecules or hydrogen that create easily evaporating tungsten oxide species. These oxide nanowhiskers then react with H_2S and H_2 gases. In the first step, a few WS_2 layers quickly form on the oxide surface. In the second step, WS_2 grows slowly inward, while oxygen diffuses outward, gradually consuming the oxide core. This "surface-inward" mechanism finally produces hollow WS_2 nanotubes. Modern high-resolution and in situ electron microscopy have confirmed this growth process.[48] [12]

2.2.2. $ReSe_2$ nanostructures

Rhenium diselenide ($ReSe_2$) is a new two-dimensional (2D) material from the family of transition metal dichalcogenides (TMDs). It has special structural and electronic properties that make it interesting for research. In $ReSe_2$, the selenium (Se) layers are located above and below the rhenium (Re) layers, forming a sandwich like structure. Unlike most TMDCs, which have a regular hexagonal structure, $ReSe_2$ has a distorted triclinic 1T structure. This distortion occurs because neighboring Re atoms bond together to form zigzag chains of four atoms, known as Re–Re chains. This arrangement makes the structure more stable and gives $ReSe_2$ its strong in-plane anisotropy.[49] [50]

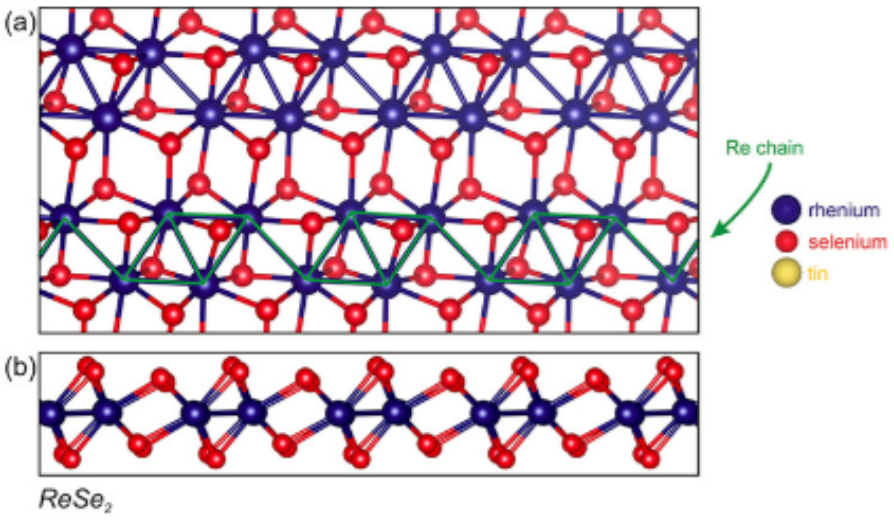

Figure 2.5.: Crystal structure of rhenium diselenide (a) along c-axis and (b) along a-axis, with marked Re-chain[4]

$ReSe_2$ is an anisotropic semiconductor, with weak van der Waals bonding between

layers that allows exfoliation into a few layers. The intensity of its Raman peaks depends strongly on the polarization of the incident laser. By rotating the laser polarization from 0 to 360 degree, it is seen that the peak intensities change periodically with a period of 180 degree, while their positions doesn't change. This strong polarization dependence confirms the anisotropic crystal structure of $ReSe_2$.[50]

$ReSe_2$ has different electronic behaviour than most transition metal dichalcogenides. Unlike most TMDCs, where the band gap changes significantly with thickness, often changing from indirect in bulk to direct in monolayers, $ReSe_2$ exhibits a nearly layer-independent band gap. This means that both thin and thick layers show similar optical transition characteristics. Although some studies reported results discussing whether the band gap is direct or indirect, most experimental and theoretical works agree that $ReSe_2$ maintains a weakly layer-dependent band gap.[51] [5] In a most recent paper, it is shown that when $ReSe_2$ becomes thinner, its bandgap changes from indirect to direct, which makes it better for light related applications. But because its structure is a little bit distorted, forming chains of atoms that cause strong anisotropy, its properties will differ depending on direction. This distortion can make the material less stable, but when stacking $ReSe_2$ with other 2D materials (to form heterostructures) it will help improve its performance.[52]

$ReSe_2$ has a triclinic unit cell, which means that there is no symmetry except the center of inversion. Its atoms are arranged in a irregular pattern and it is part of the P-1 space group.[5] It has metal-metal bonds and metal-chalcogen bonds as seen in figure 2.5 corrugated surface. Several analysis has been made for monolayers and for bulk $ReSe_2$, and from 36 vibrational modes predicted, 3 are acoustic (A_u modes), 18 are Raman active (A_g modes) and 15 are IR active modes (A_u symmetry), which are spread in the 100-300 cm^{-1} range. Raman spectra of $ReSe_2$ with different thicknesses show two main peaks: one at 124 cm^{-1} corresponding to the in-plane E_g-like mode, and another at 173 cm^{-1} corresponding to the out-of-plane A_g-like mode . Appart from these there are observed other peaks as well, between 100-300 cm^{-1}, something that is different from other TMDCs.[53] It is shown that unlike the other TMDCs, $ReSe_2$ peaks, don't shift when adding more layers, but the intensity of the peaks changes with thickness and orientation.[54] [55]

Similarly to WS_2, $ReSe_2$ can also be synthesized as a nanotube, even though, research on $ReSe_2$ nanotubes are very limited. In 2009, researchers first synthesized $ReSe_2$ nanotubes, where ammonium perrhenate was reacted with selenium nanotubes under hydrothermal conditions. In the synthesis method, the selenium nanotubes served a dual role as both reactant and structural template, directing the formation of the tubular $ReSe_2$ structure.[56]

2.2.3. Hybrid structures of WS_2 and $ReSe_2$

So far, only a few two dimensional transition metal dichalcogenides have been studied in detail, mainly MoS_2, WS_2, $MoSe_2$, and WSe_2. As a result, most heterostructure research has focused on combinations of these materials. As mentioned in Section 2.2, WS_2 is well

known among TMDs for its excellent optical properties. The electronic properties of WS_2 strongly depend on the number of layers, as is typical for TMDC materials. Bulk WS_2 is a semiconductor with an indirect band gap of about 1.3 eV, while a single (monolayer) WS_2 has a direct band gap of about 1.98 eV.[38] In contrast, as described in more details in Section 2.2.1, $ReSe_2$ is a relatively new member of the TMD family. It has a triclinic unit cell with four Re atoms forming a parallelogram-shaped cluster. Unlike other TMDCs, $ReSe_2$ shows in-plane anisotropy due to its distorted lattice structure. Another important difference from most TMDCs is that $ReSe_2$ does not undergo a transition from an indirect to a direct bandgap when thinned to a monolayer.[5] The combination of tungsten disulfide (WS_2) amd rhenium diselenide ($ReSe_2$) has been investigated in their two dimensional form, for monolayer as well as a few layers. It is a heterostructure coupled by the van der Waals force, formed by stacking a monoleyer of WS_2 on the bottom with a monolayer of $ReSe_2$ on top, as seen in Figure 2.6a). Experimental results show that the WS_2-$ReSe_2$ heterostructure exhibit type II band alignment (Figure 2.2), where electrons excited in $ReSe_2$ transfer rapidly to WS_2, while holes excited in WS_2 transfer to $ReSe_2$, as seen in Figure 2.6 b).[5]

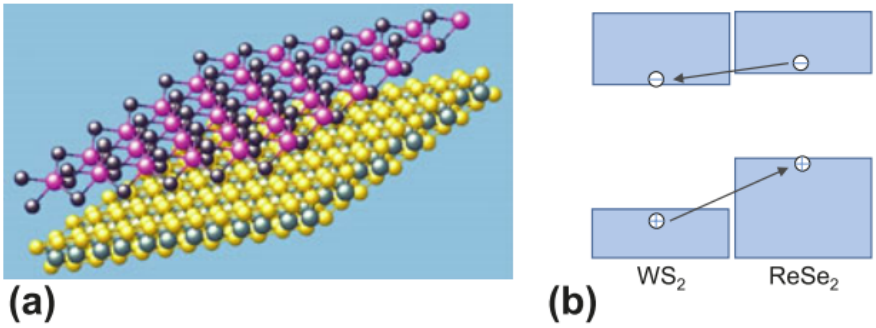

Figure 2.6.: a). The heterostructure formed by WS_2 on the bottom and $ReSe_2$ on the top. b) The band alignment of WS_2-$ReSe_2$ and the electron hole process[5]

Additionaly, for the heterostructure photoluminescence quenching is observed, which confirms efficient interlayer charge transfer. The monolayer WS_2 and the heterostructure WS_2-$ReSe_2$, were excited with a 532nm laser, at room temperature. The emission peak for both cases occurs at 615 nm, which corresponds to excitons, and the shoulder at 625nm that corresponds to trions. However, there is a decrease in intensity for the heterostructure, that is about 60%. The reduced PL in the heterostructure is likely caused by photocarriers moving from WS_2 into $ReSe_2$ before recombining.[5] Raman shifts were also observed for the $WS_2/ReSe_2$ heterostructure. For WS_2 layer, two main Raman peaks, $E_{2g}{}^1$ and A_{1g}, are identified several times at about 353.8 cm^{-1} corresponding to in-plane vibrations and 415.5 cm^{-1}, corresponding to out-of-plane vibrations. For $ReSe_2$, several Raman peaks appeared between 100 and 300 cm^{-1} due to its asymmetric crystal structure, with characteristic peaks at around 121 cm^{-1} (Eg-like) and 157 cm^{-1} (Ag-like). The Raman spectrum of the $WS_2/ReSe_2$ heterojunction shows peaks from both WS_2 and

$ReSe_2$ when these layers are stacked one on top of the other.[51]
In addition to studying the 2D $WS_2/ReSe_2$ heterostructure, this thesis explores the properties of WS_2@$ReSe_2$ nanotubes. This is a new approach to the material, and so far no information about these heteronanotubes has been reported, to my knowledge. The following chapters present the sample preparation, methods used and results from Raman spectroscopy, photoluminescence (PL) measurements, and also morphological characterization using scanning electron microscopy (SEM) combined with energy-dispersive X-ray spectroscopy (EDS). Of course, more measurements and further analysis should and will be carried out in the future to get a deeper understanding of this material.

2.3. Spectroscopy and Microscopy Methods

2.3.1. Raman spectroscopy

Raman spectroscopy is a powerful technique that provides information about vibrational properties of molecules and crystals. It is used very often, when structural, electronic, and optical properties are being studied. This method is based on the interaction between light and matter, where the scattered light contains information about the vibrational modes of the sample. The scattering happens when a particle interacts with the medium, which causes a change in its direction or energy. There are two different scatterings, elastic and inelastic. In elastic scattering the paricle is deflected from its path, but its total kinetic energy stays the same. In inelastic scattering the total energy is conserved, but the particle gains or loses energy, because the electronic states of the medium or the internal vibrations are excited.[57] [58]

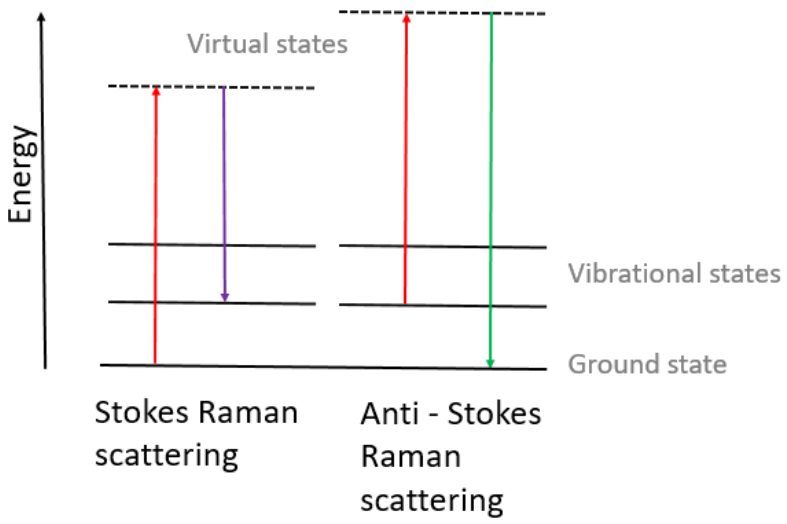

Figure 2.7.: Light can be elastically or inelastically scattered when it interacts with a material. Schematic of inelastic Raman Stokes and Anti-Stokes scattering

Raman spectroscopy is a technique based on the inelastic scattering. It was first predicted by Adolf Smekal in 1923 and later confirmed experimentally by Chandrasekhara Venkata Raman in 1928, who won the Nobel Prize in 1930. When incident photons hit the molecule, it will result in the distortion of the electron cloud. If this distortion happens only temporarily and then returns to the original state by emitting light of the same frequency as the incoming light, this is called Rayleigh scattering. In contrast to this process, where the wavelength of the incident light doesn't change after the scattering, a shift in the wavelength is observed and that is known as the Raman scattering.[57] [58] When the atom absorbs a photon, it gains energy, thus it gets excited. It then relaxes by emitting a photon. When the energy of the photon that has been emitted is lower than the energy of the photon that has been absorbed, the process is known as Stokes scattering, (see Figure 2.7). On the other hand, when the photon that gets emitted has more energy than the photon that gets absorbed, this is known as anti-Stokes scattering, (see Figure 2.7). Rayleigh scattering happens much more often than Raman scattering, which is why its signal is much stronger.[58] [57]
Raman spectroscopy has become very important for characterizing two-dimensional materials such as graphene and metal dichalcogenides, but also for nanotube structures. It provides important properties, including the number of monolayers, interlayer vibrations, and phonon modes. [59] The Raman shift is usually measured in wavenumbers.[60] Raman spectroscopy consists of a laser light source, an optical path composed of mirrors, filters, lenses and gratings, a beamspliter, a monochromator and a microscope used to focus the laser onto the sample. The scattered light is then collected and analysed by a spectrometer and a detector. [57]

2.3.2. Photoluminescence spectroscopy PL

When photons excite electrons to higher energy states, the relaxation back to lower energy states results in the emission of light, which is later analyzed.[61] It is a technique used a lot for the characterisation of the optical and the electronic properties of semiconducters. Absorption of energy and emission of light are terms which describe luminescence. If the excitation comes from electrical injection the process is called electroluminescence (EL). To create such excited electrons, the material must be excited by shining light on it. If the recombination produces light, it is called photoluminescence. In general, PL refers to the spontaneous emission of light following photoexcitation of a material. When a photon with sufficient energy is absorbed, an electron is excited from the valence band to the conduction band, leaving behind a hole. The electron–hole pair, often bound as an exciton, can also relax through different way, which can lead to recombining radiatively and emitting a photon with lower energy than the excitation source.[62] This proccess is the oposite of absorbtion spectra, instead of absorbing light to emit electrons, it emits light when electrons relax to a lower energy state.

Photoluminescence (PL) is the emission of light from a material after it absorbs photons. It is nondestructive, meaning it does not damage the sample during testing and contactless method that requires little sample preparation, since no electrical contacts are needed. Because of this, PL is used to study semiconductors. PL is important because

it is sensitive to defects, impurities, and interface roughness.[6]The choice of excitation energy and intensity is important because different energies probe different regions of the sample. The excitation energy determines two key factors: first, it selects which initial state gets excited, and second, it controls how deep the light penetrates into the material. The intensity on the othere hand is important because it controls the density of the photoexcited electrons and holes, which affect how these charge carriers behave. By changing external conditions like temperature, you can learn more about the electronic states in the material. PL has limitations as well. PL only works well with materials that emit light efficiently. Some materials for example-indirect bandgap semiconductors, have low light emission efficiency, making them difficult to study with regular PL techniques. To determine the exact number density of defects or impurities is also a challange.[6]

A typical PL setup (as seen in Figure 2.8) uses a laser as the light source, focusing optics to illuminate the sample, such as mirrors and gratings, a spectrometer and the detector to analyze the emitted light. This emitted light is collected and analyzed as a PL spectrum, which gives important information about the electronic energy levels and transitions.

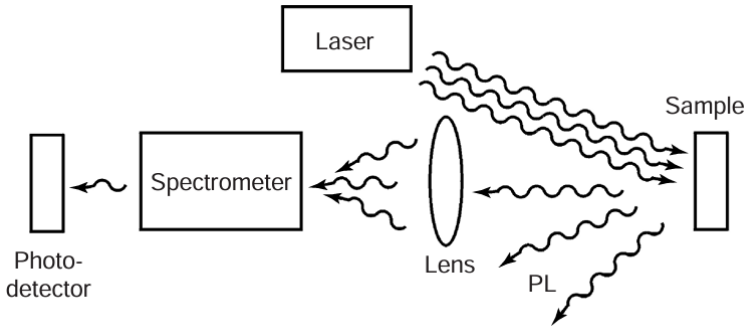

Figure 2.8.: Schematic of the PL instrumentation[6]

2.3.3. Scanning electron microscopy (SEM) and Electron dispersive X-ray spectroscopy (EDS)

Scanning electron microscopy is one of the most powerful techniques for the morphological and structural characterization of nanomaterials. It was first discovered in the 1930s and introduced in the 1960s. SEM has developed alot during the year, offering surface morphology, microstructures, etc.[63]
Scanning electron micopy operates on the fundamental principles of electron-specimen interactions to generate high resolution images. Instead of using light, SEM uses a focused beam of electrons. Because electrons have much shorter wavelengths than visible light, they can reveal details on the nanometer scale that visible light microscopes cannot. The beam is focused onto the sample surface using magnetic lenses in the microscope column,

the electron beam is generated from an electron gun and these electrons are accelerated at a certain voltage.
When the primary electron beam hits the sample,the electrons interact with atoms in the sample. These interactions happen in a small teardrop-shaped volume under the surface, as seen in the Figure 2.9. The size of this volume depends on how fast the electrons are moving and the material density. These interactions can be classified into elastic (backscattered electrons) and inelastic scattering (secondary electrons).[64] [65]

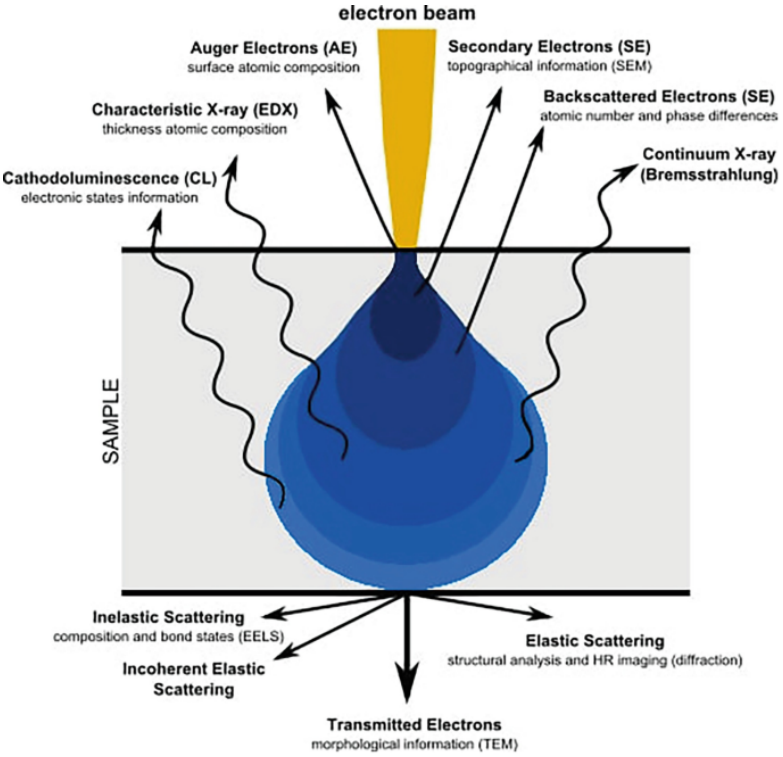

Figure 2.9.: Teardrop interaction volume of electrons with the sample[7]

Backscattered electrons (BSE) are primary beam electrons that undergo elastic scattering, while bouncing of from the positively charged nuclei with energies close to the incident beam energy. This process depends on the atomic number of the element, therefore the heavier the specimens element, the more electrons will be backscattered. Since these electrons come from a greater depth within the specimen compared with the secondary electrons (SE), they provide better compositional information.[65]
Secondary electrons (SE) are generated thorugh inelastic interactions betweem the primary electron beam and the specimen atoms and have lower energies than the BSE. The production of these electrons occurs when primary electrons transfer enough energy to valence or conduction band electrons in the specimen, ejecting them from the atom. Since these secondary electrons have low energy, they have limited escape depth, making them high-surface sensitive and ideal for high resolution topography imaging.[66] [64] A

Scanning Electron Microscope (SEM) uses a focused beam of electrons to create detailed images of the surface of the sample. The setup includes an electron gun that generates electrons, which are focused by condenser and objective lenses. Scan coils move the beam across the sample surface, while a detector collects the emitted signals (secondary or backscattered electrons). These signals are then amplified and displayed on a monitor as seen in Figure 2.10. The entire system operates under high vacuum.
Energy Dispersive X-ray Spectroscopy (EDS) is an analytical technique used for elemental analysis and chemical characterization of materials. EDS is based on the interaction between high-energy electrons and atoms in the sample. When this occurs, an electron emits a single photon, an X-ray. When an atom is irradiated by an primary electron beam, electrons get ejected from the atoms, thus holes are generated in the inner electron shells. Electrons from outer shells go to lower shells, and the extra energy is released then as X-rays. Each element produces X-rays with specific energies that are unique to that element, as the energy difference between electron shells is characteristic for each element. By detecting and measuring the energy of X-rays emitted from a sample, EDS can determine the elemental composition of the material. The detection system typically has a silicon drift detector (SDD) that converts X-ray photons into electrical signals. This method is commonly used with scanning electron microscopy (SEM).[66]

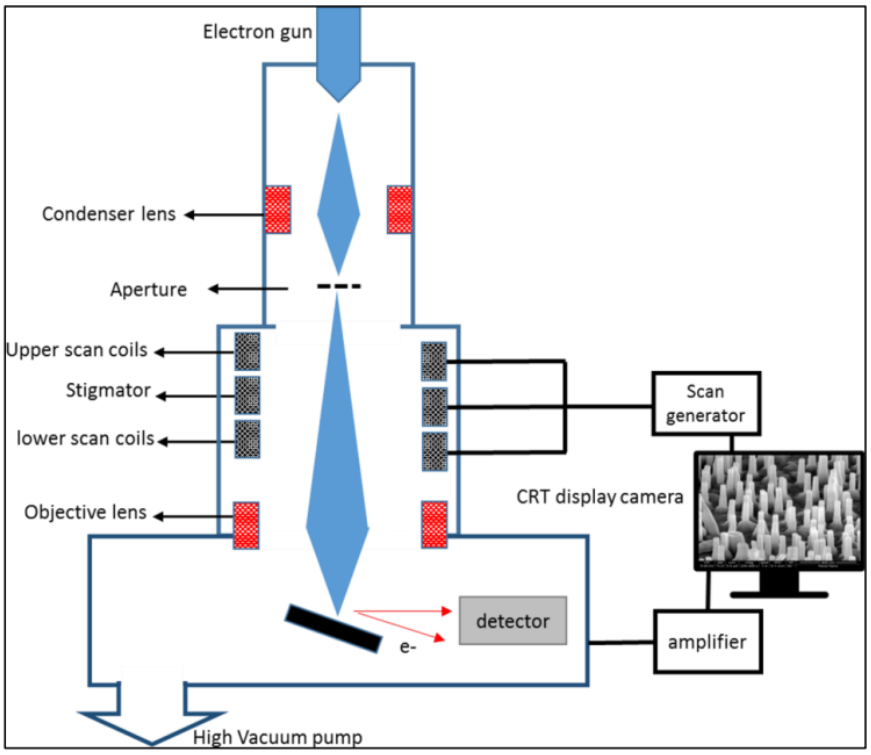

Figure 2.10.: SEM setup[8]

3. Materials and methods

This chapter describes the materials and experimental methods used in this study. It explains how the WS_2@$ReSe_2$ heterostructure nanotube samples were prepared and analyzed using different techniques. The preparation steps for scanning electron microscopy (SEM) and energy-dispersive X-ray spectroscopy (EDS), as well as photoluminescence (PL) and Raman spectroscopy,, are presented in detail. These methods were used to study the structural, optical, and vibrational properties of the WS_2@$ReSe_2$ nanotubes.

3.1. Sample Preparation Method

The precise synthesis technique of this material has not been published until the time of submission of this thesis. Therefore, in honor to our longstanding collaboration with Masaryk University and the Weizmann Institute, the details are not given. However, similar techniques have inspired and guided the development of our WS_2@$ReSe_2$ heterostructures.

3.2. Characterization Methods

The samples were received in powder form. In order to carry out the spectroscopy and microscopy characterization, specific procedures had to be considered given the characteristics of the material.

3.2.1. Scanning electron microscopy (SEM) and Energy-dispersive X-ray spectroscopy (EDS)

The piece of equipment used during this work was an Zeiss Supra 55 VP SEM operated in high vacuum. SEM is a useful technique to gain access to the overall morphology of the samples. It provides high-resolution imaging for nanoscale materials. The SEM system consists of an electron gun as the electron source, that emits a focused beam of high-energy electrons. A series of electromagnetic lenses that focus the beam, and scanning coils that direct the beam across the sample surface (a typical SEM setup is seen in figure 2.10). As the electrons interact with the sample, they undergo various scattering processes (Figure 2.9), including the generation of secondary electrons (SE) and backscattered electrons (BSE). Both secondary electron (SE) and backscattered electrons (BSE) signals were collected to study the sample surface and contrast differences. Measurements were carried out with accelerating voltages 5kV-10kV.

In addition to imaging, energy-dispersive X-ray spectroscopy (EDS) in the SEM was used to analyze the elemental composition of the samples. The EDS spectra confirmed

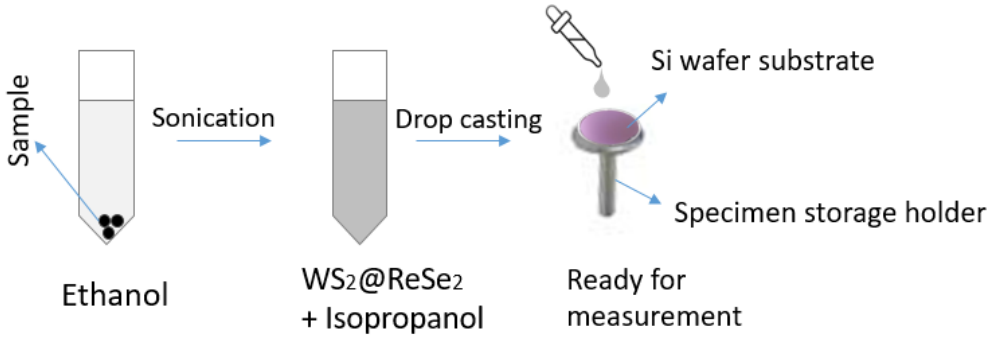

Figure 3.1.: SEM sample preparation sequence.

the presence of rhenium (Re), selenium (Se), tungsten (W), sulfur (S), verifying the composition of the WS_2@$ReSe_2$ heterostructures and identifying any possible surface contamination or impurities. Together, SEM and EDS provide structural and compositional details that are important for understanding the morphology, quality, and uniformity of the synthesized nanotubes.

For the sample preparation, a small amount of WS_2@$ReSe_2$ nanotubes in powder form was dispersed in 0.8 ml of isopropanol inside a clean sample tube (a scheme of the SEM sample preperation is seen in Figure 3.1). The dispersion was sonicated for approximately 20 minutes in an ultrasonic bath to achieve uniform suspension of the nanotubes. Meanwhile, the SiO_2 (Si substrate) were cleaned in isopropanol using the same ultrasonic bath and then dried with compressed nitrogen gas to remove any remaining moisture. Afterwards, the substrates were placed on a heating plate at 40 °C. After sonication, a few drops of WS_2@$ReSe_2$-isopropanol suspension were carefully drop-casted onto the preheated SiO_2 wafer substrate, using a micropipette. The samples were left to dry completely on the hot plate, resulting in a thin, well-distributed film of nanotubes. Once dried, the substrates were mounted onto silver SEM stubs using conductive carbon tape, to make sure the SiO_2 samples are fixed properly and to avoid charging.
This preparation method allows for uniform dispersion of nanotubes on the substrate surface, enabling high-quality SEM imaging. The obtained SEM micrographs provide information about the nanotube morphology, diameter and length, while EDS mapping confirms the overall chemical composition and spatial distribution of the constituent elements.

3.3. Photoluminescence spectroscopy

For the photoluminescence (PL) measurements in this thesis, a Horiba Jobin Yvon NanoLog spectrometer was used. The system consists of a white light source, with an excitation from 300 to 800nm, a sample chamber, a spectrometer equipped with diffraction gratings, and detectors for visible and near-infrared (NIR) signals. In this work, only the

visible-range detector was used, not the near-infrared detector.
The light source excites the sample to generate photoluminescence, which occurs when electrons in the material are excited to higher energy levels, leaving behind a positively charged vacancy, a hole, and then recombine, emitting photons. The emitted light is collected and directed through a set of mirrors and diffraction gratings into the spectrometer. The light later is detected by a photomultiplier tube (PMT) or a CCD detector. The resulting emission spectra were recorded and further analyzed using Python.

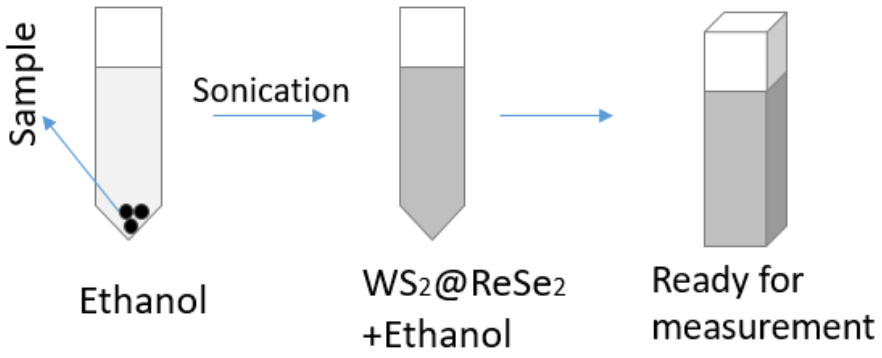

Figure 3.2.: The sample preparation for PL measurements involves ultrasonication and suspension in ethanol to ensure a uniform suspension.

For the measurements, the WS_2@$ReSe_2$ nanotube samples (powder) were first dispersed in ethanol to prepare a uniform liquid suspension ready for optical measurements. As shown in Figure 3.2, the powder sample was added to a small amount of ethanol and sonicated for one hour to break up agglomerates and to form dispersion of the nanotubes in the liquid. The resulting WS_2@$ReSe_2$–ethanol suspension was then transferred to a quartz cuvette for measurements. Material dispersion is crucial for a better PL signal. By analyzing the PL spectra,infromations about the optical bandgap can be obtained and also about interlayer interactions in the WS_2@$ReSe_2$ heteronanotubes.

3.4. Raman spectroscopy

The Raman spectrometer used in this thesis is a Horiba LabRAM HR800 system. The excitation source is a Coherent Innova 70C laser, with multiple laser excitation wavelenghts (458 nm, 488 nm, 515 nm, 532 nm, 568 nm, and 647 nm). In addition, a He–Ne laser operating at 633 nm is also coupled to the system. Figure 3.3 depicts the spectrometer configuration. Roughly summarized, while running a measurement the required laser line is chosen and it is then guided through a series of mirrors and filters in a given interferometer arrangement. Powder samples of WS_2@$ReSe_2$ nanotubes were analyzed. The samples were placed on a simple aluminum foil substrate placed on the stage beneath

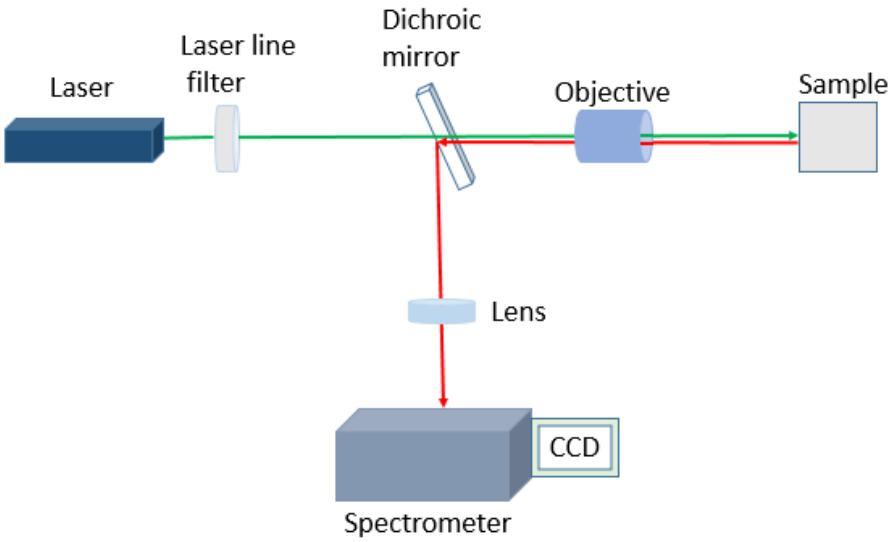

Figure 3.3.: Schematic of Raman spectrometer: After iluminating the sample, the selected beam reaches a dichroic mirror, where it reflects (green path) while allowing the Raman signal (red path) to pass through. The incident and back-scattered laser light from the same spot. The collected signal is directed to a monochromator, where it is dispersed by a diffraction grating to reach the liquid-nitrogen-cooled CCD detector.

the objective lens. Raman spectra were acquired in measurement windows of 30 s and 60 s, with 40–60 scans per window to improve signal. The obtained spectra were processed and analyzed using OriginLab software. With this Raman setup, it is possible to obtain detailed information about the vibrational modes, the quality of the sample, and interlayer coupling of the material.
A series of experiments varying the laser excitation power were performed in order to understand the response of the different layers of the tubular materials. The results obtained from these measurements are described more in depth in the next chapter.

4. Results and discussion

In this chapter, the results of the experimental measurements are presented. First, SEM-EDS analysis is shown to provide information on the morphology and elemental composition of the samples. This is followed by the photoluminescence (PL) spectra and Raman spectra, which give a brief look at the optical and vibrational properties of the material.

4.1. SEM-EDS

The SEM images were recorded to have an overall understanding of the morphology of the TMDC samples at different magnifications.
Figure 4.1a presents a SEM image recorded at an acceleration voltage of 10 kV. A large number of nanotubes can be observed, with several of them overlapping and forming clusters. However, the image also reveals the presence of flake-like structures and bulk fragments, which are unwanted byproducts of the synthesis process. These plates reduce the purity of the sample and make it more difficult to isolate well-formed nanotubes. The nanotubes in this image vary in size, with diameters ranging from about 50 to 225 nm and lengths between 815 nm and 2120 nm (2.1 µm), showing significant structural diversity. It is worth mentioning that, the majority of the nanotubes was of a larger diameter.

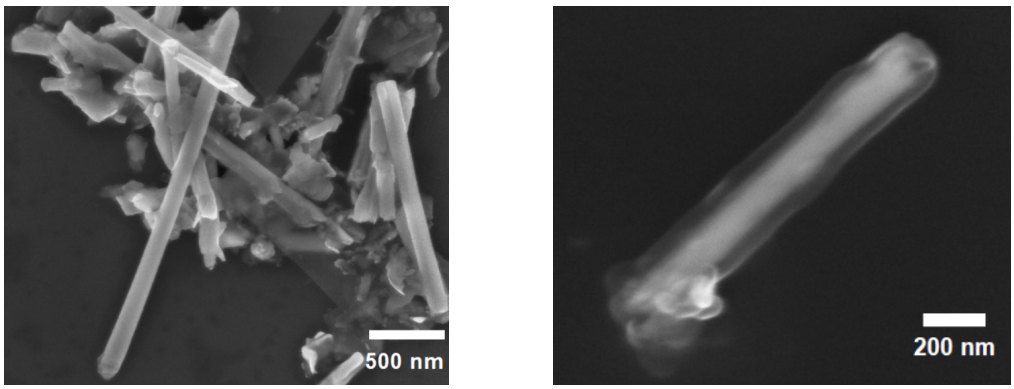

(a) Cluster of nanotubes and plates

(b) Individual long nanotube separated from bulk material

Figure 4.1.: SEM images of nanotubes. (a) shows a cluster of nanotubes and plates, while (b) shows an individual long nanotube.

Figure 4.1b (also taken at 10 kV) shows an individual nanotube separated from most

of the bulk material. This nanotube has an outer diameter of 233 nm, an inner diameter of 128 nm, and a length of 1322nm (1.32µm). Both the outer layer and a well-defined inner nanotube layer are visible. The inner layer most likely originates from the tungsten oxide precursor used during the synthesis of TMDC nanotubes. This shows the core shell structure, where the TMDC nanotbes is shell and the WO_3 indicated the core structure. At one end of the nanotube, some smaller clusters of plates are still present, suggesting incomplete separation during preparation.
Similar features appear in other SEM images, where nanotubes, plates, and bulk material are frequently found together. Figure 4.2 shows another example where a nanotube with a clear inner layer is observed. Again, it is observed the core–shell structure, which most likely consisting of a tungsten oxide nanowire inside. The presence of tungsten oxide indicates that the wanted pure nanotubes were not succesfully synthesised. To be sure that this is true, HR-TEM analysis is needed to be done. Additionaly, doing EDS analysis maybe we would be able to confirm the tungsten oxide core for this specific nanotube. However doing EDS for the specific nanotubes, we had to use around 20kV which led to the damage of the sample or even destroying the isolated nanotubes completely.

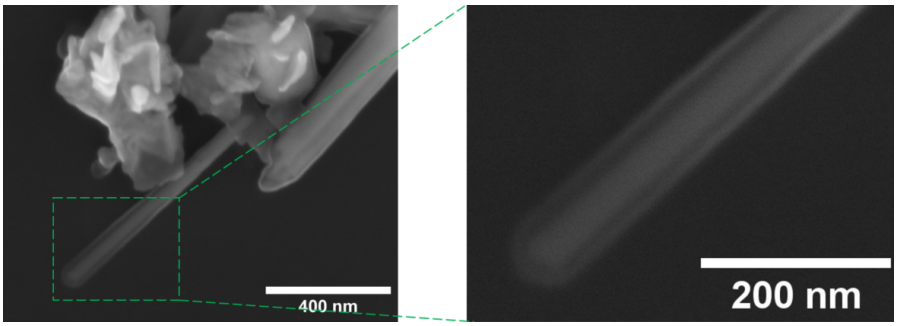

Figure 4.2.: SEM images where nanotubes as well as bulk material is seen, zoomed to a specific nanotube

From all SEM images collected (see A), the nanotubes exhibit a wide size distribution, with diameters ranging from ~ 50 to ~ 300 , but most of the nanotube diameters measured were in the range of ~ 100 nm, and lengths from ~ 800 nm to ~ 2400 nm (~ 2.4 μm). Some nanotubes appear long and well-formed, while others are shorter or partially broken. This variability confirms that the sample is structurally inhomogeneous, containing not only the desired nanotubes but also a significant fraction of plates and bulk material. Of course, the nanotubes could be broken because of the sonication process that took place for the sample preparation mentioned above.

Overall, SEM analysis show the successful formation of TMDC nanotubes, but also reveals that the sample contains impurities such as flakes and bulk material. These impurities make it difficult to achieve uniform morphology, which is important for optical measurements. To further investigate the structure and confirm the formation of clean nanotubes, higher-resolution techniques such as TEM or STEM would be valuable. Based on the SEM observations together with EDS analysis (discussed in the section below), it

is shown that the sample is composed of WS_2 or $ReSe_2$, however it's hard to say that the desired heteronanotubes needed, are found in these specific measurements.

4.1.1. Energy-dispersive X-ray spectroscopy (EDS)

The energy-dispersive X-ray spectroscopy (EDS) analysis was used together with scanning electron microscopy (SEM), to determine the chemical composition of the sample. This combined technique makes it possible to have a better understanding of the samples morphology, while looking at the elements present, which provides the materials composition. The EDS showed clear peaks of rhenium (Re), tungsten (W), and selenium (Se) and sulfur (S), confirmin the presents of our heterostructure.

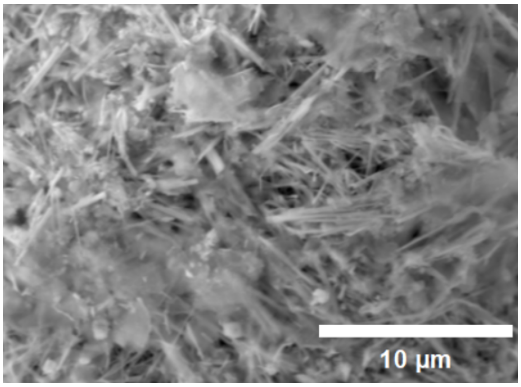

Figure 4.3.: Investigated area on the sample

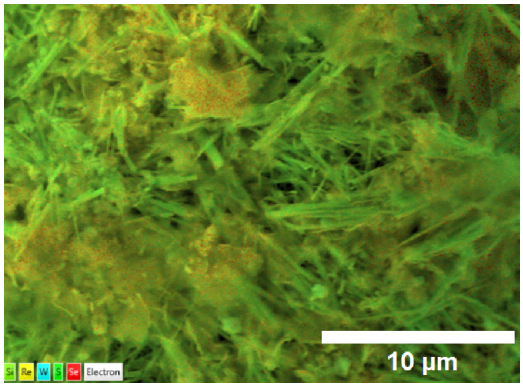

Figure 4.4.: Elemental map

Figure 4.3 shows the SEM image of the investigated area, while Figure 4.4 shows the corresponding elemental map. The EDS mapping clearly confirms the presence of tungsten (W), rhenium (Re), sulfur (S), and selenium (Se), which are the expected elements for the WS_2 and $ReSe_2$ heteronanotubes. This map shows the distribution of the main elements in the sample. The rod-shaped like materials, appear mostly in green, which corresponds to signals of S (WS_2) and also from the silicon substrate (Si) on which the sample was drop-cast, as explained in section 3.2.1. The Re and Se signals are concentrated in the bulk regions, rather than along the nanotube structures where we would want these elements to be. This indicates that the $ReSe_2$ material is mainly present in the bulk parts of the sample, while the nanotubes are mostly composed of WS_2 for this specific region.

The EDS spectrum in Figure 4.5 shows strong characteristic peaks across different energy range from 0 to 12keV, corresponding to rhenium (Re Mα), tungsten (W Mα), and selenium (Se L$\alpha_{,2}$), which represent the main elements of the $ReSe_2$ and WS_2 phases. A smaller peak corresponds to sulfur (S Kα) is also visible, confirming the presence of the WS_2 component. The silicon (Si Kα) peak comes from the SiO_2 substrate used for sample deposition. An interesting feature of the spectrum is that the Si, W and Re peaks overlap around 1.8 keV. This overlap comes from the fact that all these elements show peaks, at close energy positions. In the lower-energy region (below 1 keV), weak peaks correspond to carbon (C Kα) and oxygen (O Kα), which are likely caused by surface contamination,

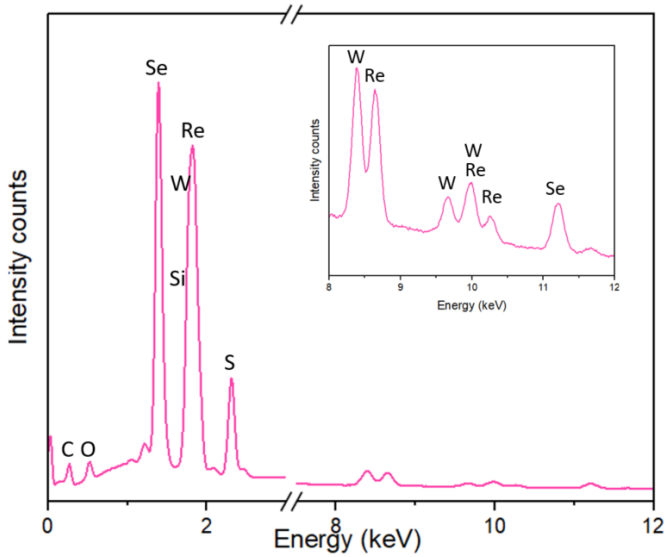

Figure 4.5.: EDS spectra of the WS_2@$ReSe_2$ nanostructures

oxidation, or the carbon tape used during sample preparation. In the same figure, we can see peaks also in the 8–12 keV range, which further confirms the presence of higher energy emission lines for W, Re, and Se. During the measurements, we tried to perform EDS on individual nanotubes, but the electron beam kept demaging the nanotubes. So we did measuments on larger area, where not only nanotubes, but bulk material can be also found. Overall, the EDS analysis confirms that the sample containes both, WS_2 and $ReSe_2$ and the overlap of W and Re peaks, together with the elemental map suggest that the two materials are integrated together, forming a connected heterostructure. However, since EDS provides only local compositional information from the near-surface region,it cannot confirm if the nanotube has a core-shell arrangement, where the one material forms the inner nanotube and the other material forms the outer nanotube. Further analysis should be done, such as TEM-EDS to see the internal structure at the nanoscale.

4.2. Photoluminescence spectra

The photoluminescence (PL) response of the WS_2@$ReSe_2$ nanotubes is seen in Figures 4.6 and 4.7. The PL map shows that the emission is strongest when the excitation wavelength is ∼365 nm, and the corresponding spectrum at this excitation displays two peaks centered at ∼405 nm and ∼425 nm as seen in Figure 4.6 (∼3 eV and ∼2.9 eV (Figure 4.7)). According to previous research, however, WS_2@$ReSe_2$ heterostructure sheets typically show PL emission under 532 nm excitation, with a main peak around 615 nm (∼2 eV). The results obtained during our measurements, are very different from those reported for the 2D heterolayered structures, both in the excitation wavelength and, more importantly, in the emission energy, which in our case lies in the blue/violet (400–425 nm)

rather than the red/orange (600–700 nm). For the shift different reasons are considered.

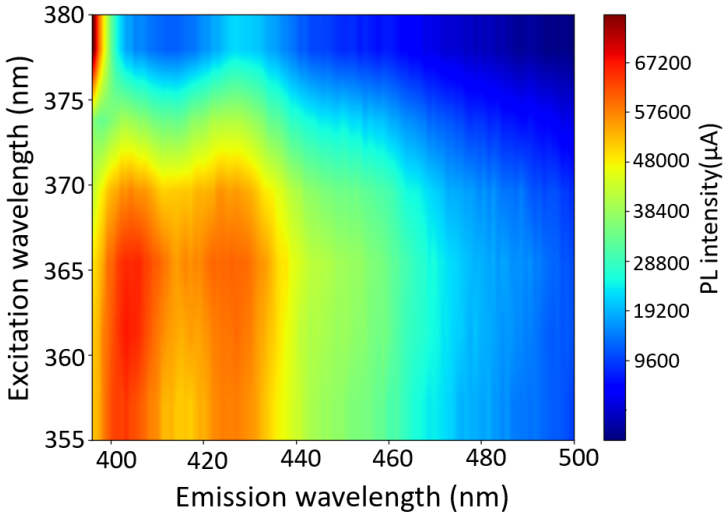

Figure 4.6.: PL map for the WS_2@$ReSe_2$ nanostructures

One of the reasons is that our sample is made of nanotubes, and not flat layers (which is the material we are comaring our results with). The curvature and interlayer coupling can shift transition energies, but such effects are generally expected to move peaks by at most a few hundred meV, so morphoology of the sample is very unlikely to be the main reason of this shift. Another reason could be that the signals might come from the solvent or even interactions between the WS_2 and $ReSe_2$ in the heterostructure could happen, that modify the emission response.
As mentioned above, when comparing with PL studies of WS_2@$ReSe_2$ layer heterostructure, the PL peak is usually reported in the range of 1.97 eV (630–690 nm)[51]. These values correspond to much longer wavelengths than the 405–425 nm emission observed here. The most likely explanation for this difference lies in instrumental issues. During the measurements, the spectrometer's detector was unstable and at times failed to register signals. This instability is probably the main reason why the emission peaks were recorded at unusually short wavelengths, instead of in the expected visible range between 600–800 nm.
Given these points and especially the detector instability, we consider that the peaks observed in these measurements (405 and 425 nm) are unlikely to represent the PL of WS_2@$ReSe_2$. The more logical reason would be that this uncertainty comes from the instrumental To make sure this true , follow-up measurements should extend the emission window to at least 350–900 nm, record background spectra from the substrate and solvent residues and measure PL under 532 nm excitation. Only after these measurments we can we say if the peaks in our measurements come from the curvature and interlayer coupling of the nanotubes or not.

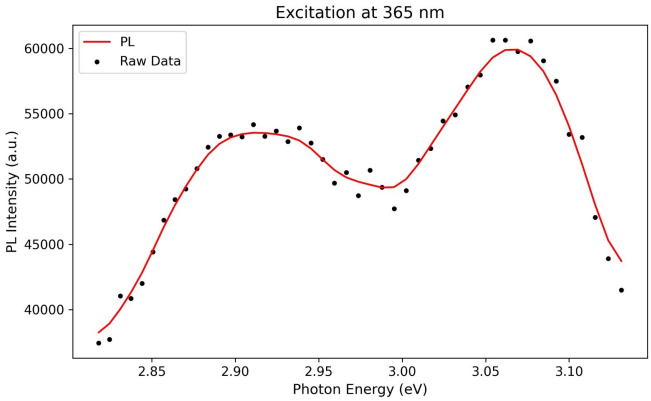

Figure 4.7.: PL graph of the emission peaks when exicted under 365nm excitation, given in eV

4.3. Raman results

Raman spectroscopy was used to investigate the vibrational properties of the WS_2@$ReSe_2$ heterostructure sample. This technique is useful for identifying the in and out of plane shifts in transition metal dichalcogenides (TMDCs). Raman was used to understand the quality of the material. Different lasers are used to investigate the sample, and measurements were also taken at various spots across the sample surface. Spectra were normalized by laser power to allow comparison of vibrational features independent of excitation intensity. Later on, the obtained results are compared with results in the literature, however, by comparing them with layered materials, since there are no results on these specific heteronanotubes.

In figure 4.8 the Raman spectra of WS_2@$ReSe_2$ nanotubes is shown. The sample is excited with the 515nm, with different laser powers. The spectra shows several peaks just as expected. The strongest peaks appear around 345.6 cm^{-1} and 412.5 cm^{-1}, each corresponds to E^1_{2g} in-plane vibrations, where atoms move paralel within the layer and A_{1g} out-of-plane vibrations, where atoms move perpendicular to the layer, respectively.These peaks are attributed to WS_2 nanotubes.[67]
From the spectrum we can also see a considerable number of peaks in the region 100-300 cm^{-1}, which correspond to $ReSe_2$. From the literature[54], for layered $ReSe_2$, the Raman peaks appear between 100 and 300 cm^{-1}, with more intense peaks at 124, 158, 284 and 294 cm^{-1}. These theoretical predictions suggest that there are up to 18 Raman active A_{1g} modes for $ReSe_2$ in this region, 15 infrared A_u modes and 3 zero frequency A_u modes. We can also compare our measured peaks with those reported for the layered $WS_2/ReSe_2$ heterostructure in the literature [51], where similar features are observed. In our measurements, the $ReSe_2$-related peaks appear in the 100–300 cm^{-1} range, consistent with its asymmetric structure, although we do not clearly observe the characteristic modes at 121 cm^{-1} (E_g-like) and 157 cm^{-1} (A_g-like) reported in the paper. For WS_2, the

main peaks are also present, but they show a noticeable shift compared to the literature values (353.82 cm^{-1} and 415.53 cm^{-1}), with a deviation of around 8.22 cm^{-1} and 3.03 cm^{-1}, respectively. This shift can be explained by differences in the sample structure, our sample consists of nanotubes, while the reference data are from layered materials. Also, depending on the thickness, the A_{1g} and E_g modes can shift up or down. Additionally, the shift might result from the lack of calibration during measurements or possible local damage to the sample caused by the high laser power.

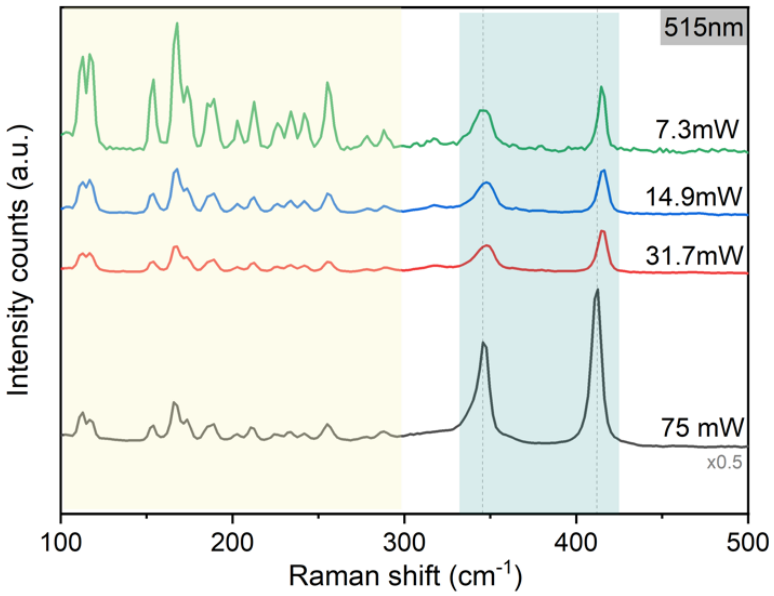

Figure 4.8.: Raman spectrum of WS_2@$ReSe_2$ nanotubes using four different filters for the 515nm

An interesting observation is seen in Figure 4.8, where we can also that for different powers, different peaks seem to be more intense. Different laser powers were used during these Raman measurements. As expected, the overall peak intensities decrease with lower excitation power, since fewer photons excite the vibrational modes. However, even at the lowest power used, the characteristic Raman peaks remain clearly visible, showing that the vibrational modes of the WS_2@$ReSe_2$ nanotubes are stable and can be detected without requiring the highest laser power. This is important because using lower power reduces the risk of heating or damaging the sample. At the same time, if we have a closer look of the spectra (Figure 4.8) we see that the peaks at low-frequency region from 100 to 300 cm^{-1}, highlighted in yellow, which contain the $ReSe_2$ related phonon modes, have higher intensity for the laser powers 7.3 mW. At high power (75 mW), these modes appear less intense compared to the 7.3mW. It is the opposite for the WS_2 peaks. It is clearly seen in the same graph, that the peaks for WS_2, highlighted in blue, when excited with the 75 mW power laser, are much higher in intensity compared to the lower power lasers. One possible reason for this behavior is that the higher laser power might have partially damaged the sample, reducing the $ReSe_2$ signal. Another reason could be

related to the focusing during the measurement, since we adjusted the focus to get higher peak intensities, it is possible that the focus was better aligned on one nanotube than the other. Also there is a tiny shift between the peaks measured, which could be from small changes in the focus or position of the laser on the sample, since the sample itself was not very clean. Another reason for these shifts to occur could be the spectrometer drift, that is why calibration for each measurement would be relevant.

More specifically, Raman spectra of a different point in the sample can be seen in Figure 4.9. A considerable number of peaks can be seen in in the region between 100-300 cm^{-1} , as well as the two main peaks of WS_2, where the E^1_{2g} mode appears at 347.6 cm^{-1}, and for A_{1g} mode the peak appears to be at 414.4 cm^{-1}. When compared with the data from the literature for WS_2 nanotubes [47] specifically, where the Raman modes are found near 352 cm^{-1} and 420.5 cm^{-1}, we can clearly see small deviations of around 4.4 cm^{-1} and 6.1 cm^{-1}. One of the main reasons for explaining these kinds of shifts is that Neon calibration or any other calibration, was not performed, and if the scale is off by even a little bit, every Raman peak will shift by the same amount. Another important reason for the shifted peaks is the nature of the sample itself. Since the measurements are taken on heteronanotubes, the curvature of the tubular geometry can influence the vibrational modes. In addition, the fact that this is a heterostructure means that WS_2 and $ReSe_2$ can interact with each other, leading to further shifts in the positions of the Raman peaks. Another possible explanation for the peak shifts is related to the sample composition and measurement conditions. From the SEM images seen in the section above, Figure 4.1a and 4.2, it is very clear that the material is not made up only by nanotubes, but also contains flakes and bulk-like regions. If the laser spot is focused on a region that is not purely nanotubes, the Raman response could be a mixture of signals from different morphologies, which can shift the peaks.

Similar measurements were done for the 633nm laser wavelength. Figures 4.10 show the Raman spectra of the WS_2@$ReSe_2$ nanotubes measured under 633 nm excitation with different laser powers ranging from 0.27 mW to 2.4 mW. The spectra shows the characteristic tungsten disulfide peaks around 350–420 cm^{-1}, which correspond to the in-plane and out-of-plane phonon modes. Additionally, several peaks appear in the lower wavenumber region between 100–300 cm^{-1} $ReSe_2$-related vibrations, as expected. This suggests that the sample structure allows us to observe signals from both the WS_2 and the $ReSe_2$ component.

At higher wavenumbers in the spectrum, strong peaks around 700 and 805 cm^{-1} appear (4.10), that are not characteristic of pristine WS_2 or $ReSe_2$ materials. These peaks are typical for W-O vibrations and indicate tungsten oxide formation. This means the WS_2@$ReSe_2$ nanotubes partly oxidized, likely due to laser heating but also maybe the process of synthesis was not finished. The detailed spectrum at 1.21 mW (Figure 4.10) shows sharp and well-defined peaks, confirming the presence of both material modes and oxide-related features.

The Raman spectra measured at 633 nm with different laser powers (4.11) show an

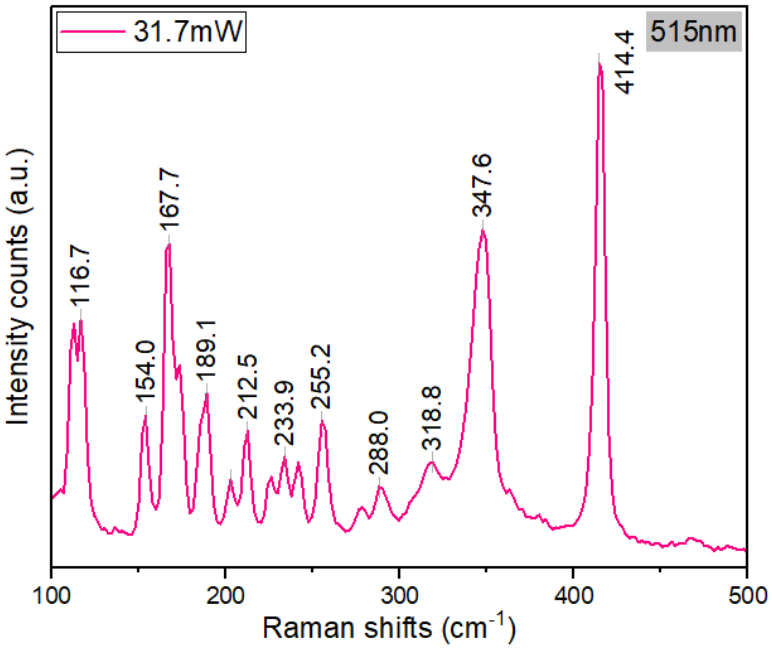

Figure 4.9.: Raman spectrum of WS_2@$ReSe_2$ nanotubes using 0.12mW power of the 515nm

unusual intensity shift. Typically, one would expect the Raman peak intensity to increase with increasing laser power. However, the experimental data shows that the peaks at 347 and 414 cm^{-1} appear more intense at a laser power of 1.21 mW compared to the higher power of 2.4 mW, as is very clearly visible in Figure 4.11. Several factors could explain this unusual intensity variation. One possible explanation could be that this difference comes from a slight change in the laser focus occurring between measurements at different powers, which would affect how efficiently the laser light interacts with the sample or even heating effects that become more pronounced at higher laser powers , which can reduce the Raman efficiency. However, based on the current data, we cannot give a proper explanation for now. More studies would be needed to fully understand this phenomenon.

In summary, the Raman measurements of WS_2@$ReSe_2$ nanotubes under different laser wavelengths and powers show the main vibrational modes clearly, but also reveal some shifts, such as unusual intensity behavior and signs of oxidation at higher powers. These results show that the heterostructure exists in our sample, but it is still hard to tell if it comes from the nanotubes itself or from the bulk part. To fully understand the observed shifts and intensity variations, more measurements and detailed analysis will be needed.

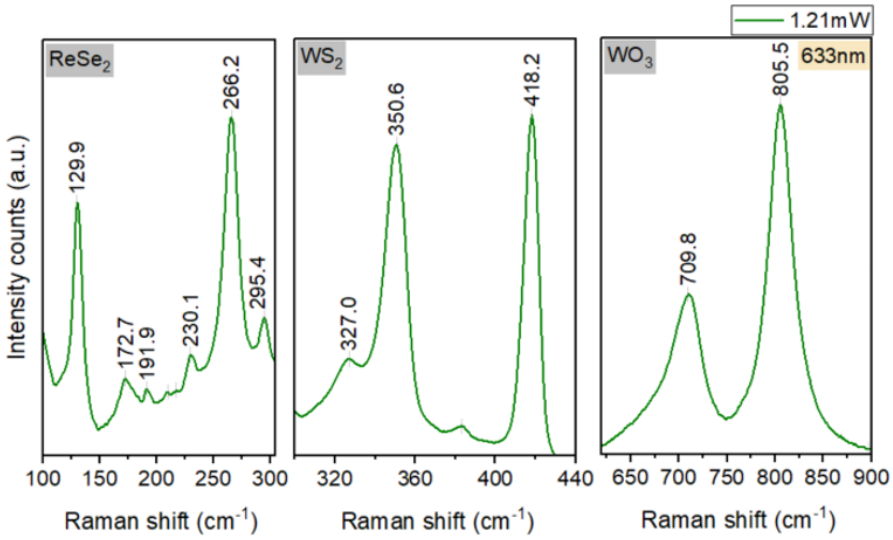

Figure 4.10.: Raman spectrum of WS_2@$ReSe_2$ nanostructures, where peaks of the heterostrctures are seen, as well as peaks from oxidation, illuminated under 633nm laser wavelength

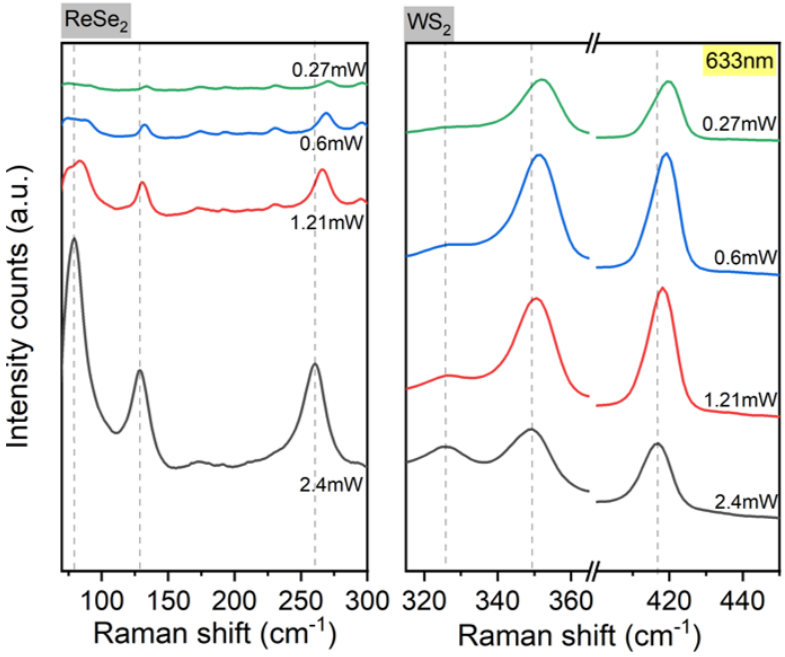

Figure 4.11.: Power-dependent Raman spectra of WS_2@$ReSe_2$ nanotubes in the 310-450 cm^{-1} region measured with 633 nm laser excitation. The spectra show characteristic Eg and Ag modes for the WS_2 nanostructure. Note the nonlinear intensity behavior where peaks at 1.21 mW (red) appear stronger than at the highest power of 2.4 mW (black)

5. Conclusion

This thesis focused on the characterization of WS_2@$ReSe_2$ heteronanotubes, a new type of material which is part of transition metal dichalcogenides (TMDCs), that has not been investigated yet. These materials are known for their unique optical and electronic properties, which can change when they are combined into heterostructures. The goal of this work was to study the optical and vibrational behavior of WS_2@$ReSe_2$ nanotubes and to understand how their tubular shape and the van der Waals interaction between the WS_2 and $ReSe_2$ layers affect their overall physical properties.

Structural and morphological analysis using scanning electron microscopy (SEM) revealed well-defined, rod-like nanotubes, clusters of nanotubes overlapping each other, and also a lot of flakes and bulk material. Energy-dispersive X-ray spectroscopy (EDS) confirmed the presence of tungsten W, rhenium Re, sulfur S, and selenium Se as the main elements, consistent with the expected WS_2 and $ReSe_2$ composition. From the elemental mapping of the specific region investigated, it was observed that the desired elements can be found in the sample, although not at the rod-shaped like part of the sample, but mostly on bulk. This means that we cannot be sure if the have the WS_2@$ReSe_2$ desired core-shell nanotubes, in the specific investigated areas on the sample. Attempts to perform EDS on individual nanotubes was hard due to beam damage of the nanotubes. To obtain a more accurate analysis of the WS_2@$ReSe_2$ heteronanotubes, it would be ideal to separate the nanotubes by centrifugation. This step would help remove unwanted bulk material and allow the measurements to focus mainly on the heteronanotubes, which are the main objective of this study.

Another method used was Raman spectroscopy which confirmed the presence of characteristic vibrational modes of both, WS_2 and $ReSe_2$, while shifts in peak positions were observed, compared to the layer form of the same materials. As reported in previous studies, the characteristic Raman peaks of $ReSe_2$ are typically found between 100–300 cm^{-1}, while the main modes of WS_2 appear around 350 cm^{-1} and 420 cm^{-1}. In our measurements, the peaks were observed in similar regions but showed slight shifts compared to the literature values. These shifts can occur for different reasons, such as interlayer coupling between the two materials or the curved geometry of the nanotubes. However, the most likely cause is the lack of calibration during the measurements, which can introduce small but noticeable deviations in the peak positions.

Photoluminescence (PL) measurements were also performed during this investigation of the material. The results for the WS_2@$ReSe_2$ nanotubes differ significantly from those reported for WS_2@$ReSe_2$ layered heterostructures. The photoluminescence spectra of the WS_2@$ReSe_2$ nanotubes showed two emission peaks at approximately 405 nm and 425 nm, which differ a lot from the literature values for layered WS_2@$ReSe_2$ heterostructures, typically around 615 nm. While this large shift could be due to the morphology of

the nanotubes or interactions between WS_2 and $ReSe_2$, it is most likely caused by instrumental instability during the measurements. The detector was unstable throughout the measurements, which likely caused the emission peaks to appear at shorter wavelengths than they should. Because of this, the PL results should be measured again to get more accurate results for WS_2@$ReSe_2$ nanotubes.

All in all, this work represents a first step toward understanding the properties of WS_2@$ReSe_2$ heteronanotubes. Although the results confirm the presence of the expected elements and vibrational modes, further improvements in sample preparation, calibration, and measurement accuracy are needed to obtain more reliable and detailed data. Future studies using cleaner, well-separated nanotube samples, together with high-resolution TEM, improved Raman and PL calibration, and theoretical modeling, will be needed to verify the core–shell structure and to better understand the optical behavior of these materials. Even though some processes should have been done differently through the sample preparation and the specific measurements, this study is a useful starting point for future research on TMDC nanotube heterostructures and their possible applications in nanotechnology and optoelectronics.

Bibliography

[1] Qing Hua Wang, Kourosh Kalantar-Zadeh, Andras Kis, Jonathan N. Coleman, and Michael S. Strano. Electronics and optoelectronics of two-dimensional transition metal dichalcogenides. *Nature Nanotechnology*, 7:699–712, 2012.

[2] Marco Bernardi, Can Ataca, Maurizia Palummo, and Jeffrey Grossman. Optical and electronic properties of two-dimensional layered materials. *Nanophotonics*, 6, 02 2017.

[3] Mitsunari Sugahara, Hideki Kawai, Yohei Yomogida, Yutaka Maniwa, Susumu Okada, and Kazuhiro Yanagi. Ambipolar transistors based on random networks of ws 2 nanotubes. *Applied Physics Express*, 9:075001, 06 2016.

[4] A Taube, A Łapińska, J Judek, and M Zdrojek. Temperature dependence of raman shifts in layered ReSe2 and SnSe2 semiconductor nanosheets. *Appl. Phys. Lett.*, 107(1):013105, July 2015.

[5] Xiuxiu Han, Dawei He, Lu Zhang, Shengcai Hao, Shuangyan Liu, Jialu Fu, Qing Miao, Jiaqi He, Yongsheng Wang, and Hui Zhao. Type-ii ws_2–$rese_2$ heterostructure and its charge-transfer properties. *Journal of Materials Research*, 35(11):1417–1423, 2020.

[6] Timothy Gfroerer. *Photoluminescence in Analysis of Surfaces and Interfaces*. 09 2006.

[7] Atria Innovation. Scanning electron microscopy: Uses. https://atriainnovation.com/en/blog/scanning-electron-microscopy-uses/. Accessed: 15 Oct. 2025.

[8] Tahani Flemban. *High Quality Zinc Oxide Thin Films and Nanostructures prepeated by Pulsed Laser Deposition for Photodetectors*. PhD thesis, 01 2018.

[9] Sajedeh Manzeli, Dmitry Ovchinnikov, Diego Pasquier, Oleg V Yazyev, and Andras Kis. 2D transition metal dichalcogenides. *Nat. Rev. Mater.*, 2(8):17033, June 2017.

[10] Wenyu Zhao, Zohreh Ghorannevis, Lain-Jong Chu, Minglin Toh, Christian Kloc, Ping-Heng Tan, and Goki Eda. Evolution of electronic structure in atomically thin sheets of ws_2 and wse_2. *ACS Nano*, 7(1):791–797, January 2013. PMID: 23256505.

[11] Min Wu, Yonghong Xiao, Yang Zeng, Yuanliang Zhou, Xiangbin Zeng, Lining Zhang, and Wugang Liao. Synthesis of two-dimensional transition metal dichalcogenides for electronics and optoelectronics. *InfoMat*, 3(4):362–396, April 2021.

[12] Lena Yadgarov and Reshef Tenne. Nanotubes from transition metal dichalcogenides: Recent progress in the synthesis, characterization and electrooptical properties. *Topics in Current Chemistry*, 375(4):1–30, 2017.

[13] Jeffrey D. Cain, Eve D. Hanson, Fengyuan Shi, and Vinayak P. Dravid. Emerging opportunities in the two-dimensional chalcogenide systems and architecture. *Current Opinion in Solid State and Materials Science*, 20(6):374–387, 2016. the COSSMS Twentieth Anniversary Issue.

[14] Samata Jain, Ravi Trivedi, Jeetendra Kumar Banshiwal, AS Singh, and Brahmananda Chakraborty. Two-dimensional materials (2dms): Classification, preparations, functionalization and fabrication of 2dms-oriented electrochemical sensors. In *2D Materials-Based Electrochemical Sensors*, pages 45–132. Elsevier, 2023.

[15] Yang Fu, Yuan Liao, Peng Li, Hui Li, Shuaiyu Jiang, Hongwei Huang, Wenping Sun, Tianyan Li, Hai Yu, Kangkang Li, Hao Li, Baohua Jia, and Tianyi Ma. Layer structured materials for ambient nitrogen fixation. *Coordination Chemistry Reviews*, 460:214468, 2022.

[16] Abdul Majid and Alia Jabeen. Transition metal dichalcogenides—an important class of layered materials. In *Layeredness in Materials: Characteristics, Strategies and Applications*, pages 103–140. Springer, 2023.

[17] Ganesh Ghimire, Krishna P Dhakal, Wooseon Choi, Yonas Assefa Esthete, Seon Je Kim, Trang Thu Tran, Hyoyoung Lee, Heejun Yang, Dinh Loc Duong, Young-Min Kim, et al. Doping-mediated lattice engineering of monolayer res2 for modulating in-plane anisotropy of optical and transport properties. *ACS nano*, 15(8):13770–13780, 2021.

[18] Jong Hun Kim, Hayeong Sung, and Gwan-Hyoung Lee. Phase engineering of two-dimensional transition metal dichalcogenides. *Small Science*, 4(1):2300093, 2024.

[19] Rafael Roldán, Andrés Castellanos-Gomez, Emmanuele Cappelluti, and Francisco Guinea. Strain engineering in semiconducting two-dimensional crystals. *Journal of Physics: Condensed Matter*, 27(31):313201, 2015.

[20] Alberto Taffelli, Sandra Dirè, Alberto Quaranta, and Lucio Pancheri. Mos2 based photodetectors: a review. *Sensors*, 21(8):2758, 2021.

[21] Faguang Yan, Ce Hu, Ziao Wang, Hailong Lin, and Kaiyou Wang. Perspectives on photodetectors based on selenides and their van der waals heterojunctions. *Applied Physics Letters*, 118(19), 2021.

[22] Arnab Pal, Shuo Zhang, Tanmay Chavan, Kunjesh Agashiwala, Chao-Hui Yeh, Wei Cao, and Kaustav Banerjee. Quantum-engineered devices based on 2d materials for next-generation information processing and storage. *Advanced Materials*, 35(27):2109894, 2023.

[23] Mikko Turunen, Mauro Brotons-Gisbert, Yunyun Dai, Yadong Wang, Eleanor Scerri, Cristian Bonato, Klaus D Jöns, Zhipei Sun, and Brian D Gerardot. Quantum photonics with layered 2d materials. *Nature Reviews Physics*, 4(4):219–236, 2022.

[24] Mehran Kianinia, Zai-Quan Xu, Milos Toth, and Igor Aharonovich. Quantum emitters in 2d materials: Emitter engineering, photophysics, and integration in photonic nanostructures. *Applied Physics Reviews*, 9(1), 2022.

[25] Wei Chen, Elton JG Santos, Wenguang Zhu, Efthimios Kaxiras, and Zhenyu Zhang. Tuning the electronic and chemical properties of monolayer mos2 adsorbed on transition metal substrates. *Nano letters*, 13(2):509–514, 2013.

[26] Krishna Kiran Pawar, Ashok Kumar, Ali Mirzaei, Mahesh Kumar, Hyoun Woo Kim, and Sang Sub Kim. 2d nanomaterials for realization of flexible and wearable gas sensors: A review. *Chemosphere*, 352:141234, 2024.

[27] Qingsheng Zeng, Hong Wang, Wei Fu, Yongji Gong, Wu Zhou, Pulickel M Ajayan, Jun Lou, and Zheng Liu. Band engineering for novel two-dimensional atomic layers. *Small*, 11(16):1868–1884, 2015.

[28] Xin Zhang, Xiao-Fen Qiao, Wei Shi, Jiang-Bin Wu, De-Sheng Jiang, and Ping-Heng Tan. Phonon and raman scattering of two-dimensional transition metal dichalcogenides from monolayer, multilayer to bulk material. *Chemical Society Reviews*, 44(9):2757–2785, 2015.

[29] Henan Li, Yumeng Shi, Ming-Hui Chiu, and Lain-Jong Li. Emerging energy applications of two-dimensional layered transition metal dichalcogenides. *Nano Energy*, 18:293–305, 2015.

[30] Davi Marcelo Soares, Santanu Mukherjee, and Gurpreet Singh. Tmds beyond mos2 for electrochemical energy storage. *Chemistry–A European Journal*, 26(29):6320–6341, 2020.

[31] Shahzadi Noreen, Muhammad Bilal Tahir, Abid Hussain, T Nawaz, Jalil Ur Rehman, A Dahshan, Meshal Alzaid, and Hussein Alrobei. Emerging 2d-nanostructured materials for electrochemical and sensing application-a review. *International Journal of Hydrogen Energy*, 47(2):1371–1389, 2022.

[32] Li Wei, Chen Jun-fang, He Qinyu, and Wang Teng. Electronic and elastic properties of mos2. *Physica B: Condensed Matter*, 405(10):2498–2502, 2010.

[33] Nitin Choudhary, Chao Li, Hee-Suk Chung, Julian Moore, Jayan Thomas, and Yeonwoong Jung. High-performance one-body core/shell nanowire supercapacitor enabled by conformal growth of capacitive 2d ws2 layers. *ACS nano*, 10(12):10726–10735, 2016.

[34] Jing Cao, Yicen Zhang, Cen Zhang, Lejuan Cai, Zelong Li, and Congshan Zhou. Construction of defect-rich 1t-mos2 towards efficient electrocatalytic hydrogen evolution: recent advances and future perspectives. *Surfaces and Interfaces*, 25:101305, 2021.

[35] Nicholas Rono, Chinedu Christian Ahia, and Edson Leroy Meyer. Recent advances in transition metal dichalcogenides-based materials for fourth-generation perovskite solar cell devices. *AIP Advances*, 14(7):070702, 07 2024.

[36] Philipp Nagler, Fabian Mooshammer, Jens Kunstmann, Mariana V Ballottin, Anatolie Mitioglu, Alexey Chernikov, Andrey Chaves, Frederick Stein, Nicola Paradiso, Sebastian Meier, Gerd Plechinger, Christoph Strunk, Rupert Huber, Gotthard Seifert, David R Reichman, Peter C M Christianen, Christian Schüller, and Tobias Korn. Interlayer excitons in transition-metal dichalcogenide heterobilayers. *Phys. Status Solidi B Basic Res.*, 256(12):1900308, December 2019.

[37] Jed Kistner-Morris, Ao Shi, Erfu Liu, Trevor Arp, Farima Farahmand, Takashi Taniguchi, Kenji Watanabe, Vivek Aji, Chun Hung Lui, and Nathaniel Gabor. Electric-field tunable type-i to type-ii band alignment transition in $mose_2/ws_2$ heterobilayers. *Nature Communications*, 11(1):3606, 2020.

[38] Pangihutan Gultom, Jiang-Yan Chiang, Tzu-Tai Huang, Jung-Chuan Lee, Shu-Hsuan Su, and Jung-Chung Andrew Huang. Structural and optical properties of tungsten disulfide nanoscale films grown by sulfurization from w and wo3. *Nanomaterials*, 13(7), 2023.

[39] Ana Laura Elías, Néstor Perea-López, Andrés Castro-Beltrán, Ayse Berkdemir, Ruitao Lv, Simin Feng, Aaron D. Long, Takuya Hayashi, Yoong Ahm Kim, Morinobu Endo, Humberto R. Gutiérrez, Nihar R. Pradhan, Luis Balicas, Thomas E. Mallouk, Florentino López-Urías, Humberto Terrones, and Mauricio Terrones. Controlled synthesis and transfer of large-area ws2 sheets: From single layer to few layers. *ACS Nano*, 7(6):5235–5242, 2013. PMID: 23647141.

[40] S Ghosh, V Brüser, I Kaplan-Ashiri, R Popovitz-Biro, S Peglow, J I Martínez, J A Alonso, and A Zak. Cathodoluminescence in single and multiwall WS2 nanotubes: Evidence for quantum confinement and strain effect. *Appl. Phys. Rev.*, 7(4):041401, December 2020.

[41] Ruilong Yang, Shanghuai Feng, Xunyong Lei, Xiaoyu Mao, Anmin Nie, Bochong Wang, Kun Luo, Jianyong Xiang, Fusheng Wen, Congpu Mu, Zhisheng Zhao, Bo Xu, Hualing Zeng, Yongjun Tian, and Zhongyuan Liu. Effect of layer and stacking sequence in simultaneously grown 2h and 3r ws2 atomic layers. *Nanotechnology*, 30(34):345203, jun 2019.

[42] Ayse Berkdemir, Humberto R Gutiérrez, Andrés R Botello-Méndez, Néstor Perea-López, Ana Laura Elías, Chen-Ing Chia, Bei Wang, Vincent H Crespi, Florentino

López-Urías, Jean-Christophe Charlier, Humberto Terrones, and Mauricio Terrones. Identification of individual and few layers of WS2 using raman spectroscopy. *Sci. Rep.*, 3(1), April 2013.

[43] A. Rothschild, R. Popovitz-Biro, O. Lourie, and R. Tenne. Morphology of multiwall ws2 nanotubes. *The Journal of Physical Chemistry B*, 104(38):8976–8981, 2000.

[44] Jun Chen, Suo-Long Li, Feng Gao, and Zhan-Liang Tao. Synthesis and characterization of ws2 nanotubes. *Chemistry of Materials*, 15(4):1012–1019, 2003.

[45] Md Ashiqur Rahman, Yohei Yomogida, Abdul Ahad, Kan Ueji, Mai Nagano, Akane Ihara, Hiroyuki Nishidome, Mikito Omoto, Shigeki Saito, Yasumitsu Miyata, Yanlin Gao, Susumu Okada, and Kazuhiro Yanagi. es of WS2 nanotubes with relatively small diameters. *Sci. Rep.*, 13(1):16959, October 2023.

[46] Vojtěch Kundrát, Rita Rosentsveig, Kristýna Bukvišová, Daniel Citterberg, Miroslav Kolíbal, Shachar Keren, Iddo Pinkas, Omer Yaffe, Alla Zak, and Reshef Tenne. Submillimeter-long ws2 nanotubes: The pathway to inorganic buckypaper. *Nano Letters*, 23(22):10259–10266, 2023. PMID: 37805929.

[47] Xiao Hu Wang, Chang Cheng Zheng, and Ji Qiang Ning. Influence of curvature strain and van der waals force on the inter-layer vibration mode of WS2 nanotubes: A confocal micro-raman spectroscopic study. *Sci. Rep.*, 6(1), September 2016.

[48] Vojtěch Kundrát, Libor Novák, Kristýna Bukvišová, Jakub Zálešák, Eva Kolíbalová, Rita Rosentsveig, M.B. Sreedhara, Hila Shalom, Lena Yadgarov, Alla Zak, Miroslav Kolíbal, and Reshef Tenne. Mechanism of ws2 nanotube formation revealed by in situ/ex situ imaging. *ACS Nano*, 18(19):12284–12294, 2024. PMID: 38698720.

[49] Bhakti Jariwala, Damien Voiry, Apoorv Jindal, Bhagyashree A. Chalke, Rudheer Bapat, Arumugam Thamizhavel, Manish Chhowalla, Mandar Deshmukh, and Arnab Bhattacharya. Synthesis and characterization of res2 and rese2 layered chalcogenide single crystals. *Chemistry of Materials*, 28(10):3352–3359, 2016.

[50] Huan Zhao, Jiangbin Wu, Hongxia Zhong, Qiushi Guo, Xiaomu Wang, Fengnian Xia, Li Yang, Pingheng Tan, and Han Wang. Interlayer interactions in anisotropic atomically thin rhenium diselenide. *Nano Research*, 8(11):3651–3661, Oct 2015_10.

[51] Changhui Du, Honglei Gao, Yurun Sun, Meixuan Liu, Jianfei Li, Jie Sun, Jiancai Leng, Wenjia Wang, and Kuilong Li. High-performance self-driven ultraviolet-visible photodetector based on type-ii ws2/rese2 van der waals heterostructure. *Journal of Alloys and Compounds*, 976:173122, 2024.

[52] Zhihao Zhang, Yang Zhang, Ling-Xiu Chen, Xiaoxiao Wang, Shenbo Zhu, Yue Yu, Xiao-Lan Xue, Chuan-Lei Jia, and Li-Wei Shi. Heterostructure-induced modulation of optical anisotropy in ReSe2. *Appl. Phys. Lett.*, 126(13), March 2025.

[53] Wuhong Xue, Peng Wang, Wenjuan Ci, Ying Guo, Jingyuan Qu, Zeting Zeng, Tianqi Liu, Ri He, Shaobo Cheng, and Xiaohong Xu. Emergence of sliding ferroelectricity in naturally parallel-stacked multilayer ReSe2 semiconductor. *Nat. Commun.*, 16(1):6313, July 2025.

[54] Daniel Wolverson, Simon Crampin, Asieh S. Kazemi, Adelina Ilie, and Simon J. Bending. Raman spectra of monolayer, few-layer, and bulk rese2: An anisotropic layered semiconductor. *ACS Nano*, 8(11):11154–11164, 2014. PMID: 25365239.

[55] Volodymyr O Yukhymchuk, Leonid M Kulikov, Mykhailo Y Valakh, Alexander P Litvinchuk, Mykola A Skoryk, Nazar V Mazur, Volodymyr S Yefanov, Oleksandr Selyshchev, Volodymyr M Dzhagan, and Dietrich R T Zahn. Structure and vibrational spectra of ReSe 2 nanoplates. *J. Raman Spectrosc.*, 51(8):1305–1314, August 2020.

[56] David Seley, Manashi Nath, and Bruce Parkinson. Rese2 nanotubes synthesized from sacrificial templates. *Journal of Materials Chemistry - J MATER CHEM*, 19, 03 2009.

[57] Hans Kuzmany. *Solid-state spectroscopy.* Springer, Berlin, Germany, 2 edition, November 2009.

[58] Ado Jorio, Mildred S Dresselhaus, Riichiro Saito, and Gene Dresselhaus. *Raman Spectroscopy in Graphene Related Systems.* Wiley-VCH Verlag, Weinheim, Germany, January 2011.

[59] Robin R. Jones, David C. Hooper, Liwu Zhang, Daniel Wolverson, and Ventsislav K. Valev. Raman techniques: Fundamentals and frontiers. *Nanoscale Research Letters*, 14(1):231, 2019.

[60] Dheeraj Kumar Singh, Manik Pradhan, and Arnulf Materny, editors. *Modern Techniques of Spectroscopy: Basics, Instrumentation, and Applications.* Progress in Optical Science and Photonics. Springer, Cham, 2021.

[61] Mike Tebyetekerwa, Jian Zhang, Zhen Xu, Thien N. Truong, Zongyou Yin, Yuerui Lu, Seeram Ramakrishna, Daniel Macdonald, and Hieu T. Nguyen. Mechanisms and applications of steady-state photoluminescence spectroscopy in two-dimensional transition-metal dichalcogenides. *ACS Nano*, 14(11):14579–14604, 2020. PMID: 33155803.

[62] Peter Y. Yu and Manuel Cardona. *Fundamentals of Semiconductors: Physics and Materials Properties.* Springer, Berlin, Heidelberg, 4 edition, 2010.

[63] Joseph Goldstein, Dale E. Newbury, Joseph R. Michael, Patrick Echlin, Eric Lifshin, Linda Sawyer, and J.R. Michael. *Scanning Electron Microscopy and X-Ray Microanalysis.* Springer, 4 edition, 2018.

[64] Anwar Ul-Hamid. *A beginners' guide to scanning electron microscopy.* Springer International Publishing, Cham, Switzerland, 1 edition, November 2018.

[65] Joseph I. Goldstein, Dale E. Newbury, Joseph R. Michael, Nicholas W. M. Ritchie, John Henry J. Scott, and David C. Joy. *Backscattered Electrons*, pages 15–28. Springer New York, New York, NY, 2018.

[66] Ana Violeta Girão, Gianvito Caputo, and Marta C. Ferro. Chapter 6 - application of scanning electron microscopy–energy dispersive x-ray spectroscopy (sem-eds). In Teresa A.P. Rocha-Santos and Armando C. Duarte, editors, *Characterization and Analysis of Microplastics*, volume 75 of *Comprehensive Analytical Chemistry*, pages 153–168. Elsevier, 2017.

[67] Vojtech Kundrat, Emil Parth, Ramon Pinna Brito, Hila Shalom, Philip Immanuel, Jakub Zalesak, Lothar Houben, Anna Kossoy, Lena Yadgarov, Paola Ayala, and Reshef Tenne. Epitaxial assembly and spectroscopic inspection of core–shell ws2@wse2 nanotubes. *Chemistry of Materials*, 37(15):5966–5973, 2025.

A. Appendix

A.1. SEM images

This section includes additional SEM images of the WS2@rese2 samples that support the results discussed in the main text. The images show different magnifications and morphology of the nanostructures, including clusters, individual nanotubes, and mixed rod–flake formations. These images provide a clearer view of the surface sample, where is seen that the samples are not made purely by the desired nanotubes.

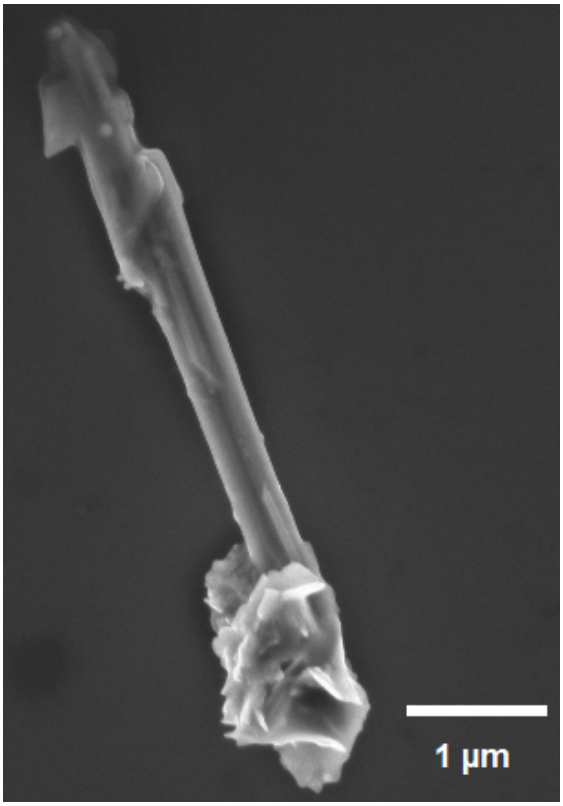

Figure A.1.: SEM images of an isolated nanotube, with a bulk part on the tip of the nanotube. EHT = 5 kV

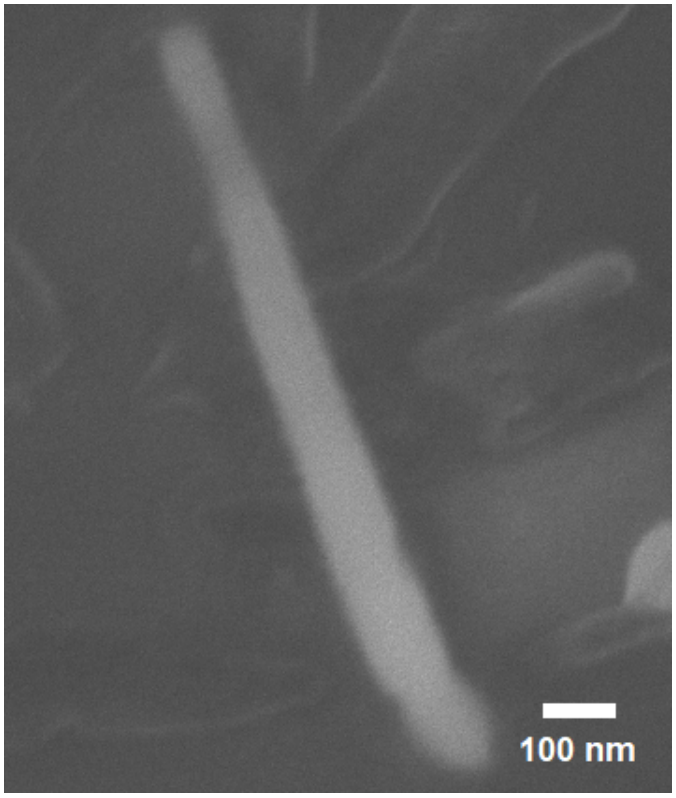

Figure A.2.: High-magnification SEM image showing a thin nanotube. The tube has a uniform shape and a diameter close to 100 nm. EHT = 5 kV.

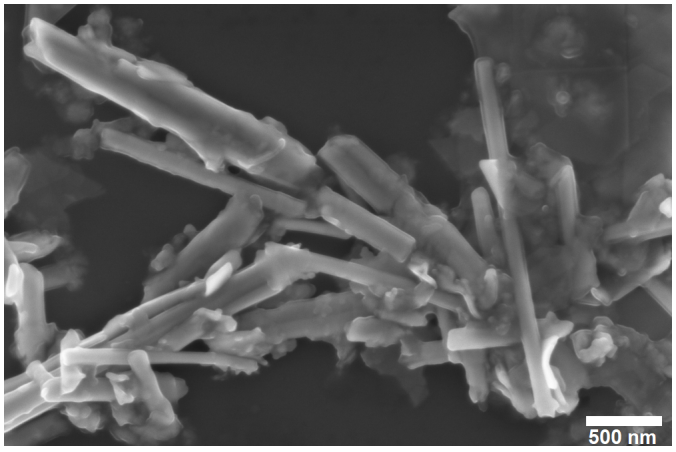

Figure A.3.: SEM image of WS2@ReSe nanostructures. It is clearly seen that there is a clusters of nanotubes, partly covered with smaller particles, showing that different shapes were formed during synthesis and that the sample it is not pure nanotubes. EHT = 5 kV

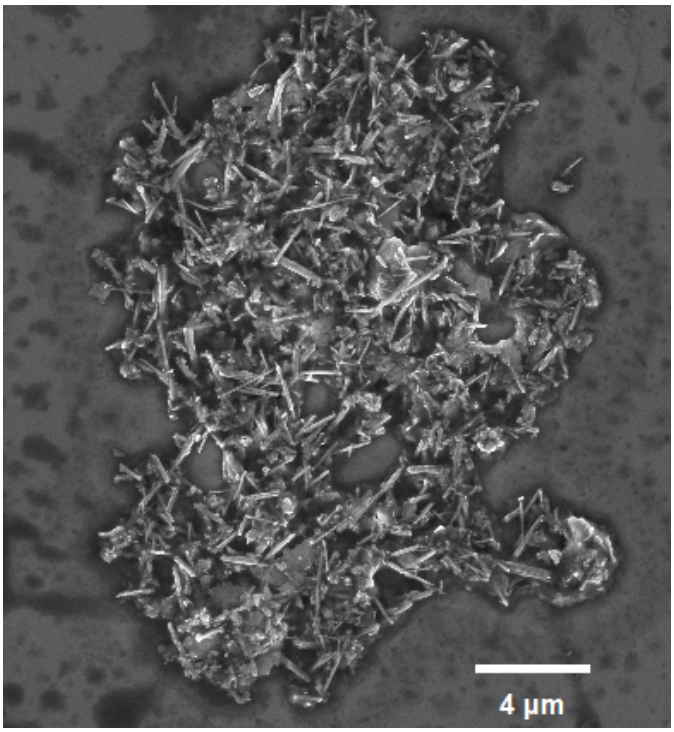

Figure A.4.: SEM image of WS2@ReSe2 nanostructures showing an agglomerated cluster of nanosheets and short rods. EHT = 5 kV